Lithos 227 (2015) 241–254

Contents lists available at ScienceDirect

Lithos

journal homepage: www.elsevier.com/locate/lithos

Role of asthenosphere and lithosphere in the genesis of the Early Permian Huangshan mafic–ultramafic intrusion in the Northern Tianshan, NW China

Yu-Feng Deng [a], Xie-Yan Song [b,*], Pete Hollings [a,c], Taofa Zhou [a], Feng Yuan [a], Lie-Meng Chen [b], Dayu Zhang [a]

[a] School of Resources and Environmental Engineering, Hefei University of Technology, Hefei 230009, China
[b] State Key Laboratory of Ore Deposit Geochemistry, Institute of Geochemistry, Chinese Academy of Sciences, Guiyang 550002, China
[c] Department of Geology, Lakehead University, 955 Oliver Road, Thunder Bay, ON P7B 5E1, Canada

ARTICLE INFO

Article history:
Received 17 December 2014
Accepted 10 April 2015
Available online 26 April 2015

Keywords:
Huangshan mafic–ultramafic intrusion
Tarim mantle plume
Slab break-off
Metasomatized mantle
Asthenospheric melts

ABSTRACT

The Huangshan mafic–ultramafic intrusion hosts a large Ni–Cu sulfide deposit and is situated in the Northern Tianshan at the southern margin of the Central Asian Orogenic Belt (CAOB). The Early Permian intrusion consists of lherzolite, websterite, gabbronorite, gabbro and diorite. The Huangshan deposit contains ~80.4 Mt of ore grading 0.54 wt.% Ni and 0.3 wt.% Cu and is the second largest magmatic sulfide deposit in Northern Xinjiang, China. The Huangshan intrusive rocks are enriched in large ion lithophile elements and depleted in high field strength elements relative to N-MORB, with low Nb/U (1.53–5.27) and high Ba/Nb (1.68–121) ratios, indicating that the primary magma was derived from partial melting of a metasomatized mantle source. The mafic–ultramafic rocks in the Northern Tianshan are characterized by lower Ca contents (<1000 ppm) in olivine, more depleted Nb and Ta, lower Nb/U ratios, and higher $\varepsilon Nd_{(t)}$ than those of the Tarim mafic–ultramafic intrusive rocks and ocean island basalts (OIB). The range of $\varepsilon Nd_{(t)}$ values of the mafic–ultramafic rocks in the Northern Tianshan over time suggests a greater role for upwelling asthenospheric mantle in the younger rocks. This implies that they were produced by interactions between metasomatized lithospheric mantle and depleted asthenospheric melts rather than a mantle plume. The linear distribution of Permian mafic–ultramafic intrusions along the Kangguer fault in the Northern Tianshan suggests that slab breakoff played a key role in the genesis of the mantle-derived magma in a syn-collisional setting.

1. Introduction

The Northern Tianshan of the Central Asian Orogenic Belt (CAOB) is host to numerous small Permian mafic–ultramafic intrusions. These intrusions provide a natural laboratory to investigate the nature of the tectonic event that triggered mantle-derived magmatism. Although it is generally accepted that subduction-modified lithospheric mantle was involved in the formation of the primary magma for these intrusions, there is controversy as to what caused the partial melting of metasomatized mantle (Deng et al., 2011a,b, 2014; Gao and Zhou, 2013; Q.G. Mao et al., 2014, Song et al., 2011, 2013; Su et al., 2012; Sun et al., 2013a,b; Tang et al., 2013; Y.J. Mao et al., 2014). Xiao et al. (2004, 2009), Han et al. (2010) and Q.G. Mao et al. (2014) have proposed that the mafic–ultramafic rocks represent Alaskan-type intrusions produced by either oblique subduction or ridge subduction. Others have attributed the formation of the mafic–ultramafic intrusions to magmatism triggered by slab break-off in a syn- or post-collisional tectonic setting (Chen et al., 2011; Deng et al., 2014; Gao and Zhou, 2013; Gu et al., 2006; Mao et al., 2008; Song et al., 2013; Yuan et al., 2010). It has also been argued, based on the similar ages of Permian igneous rocks in the Northern Tianshan belt and the Tarim Large Igneous Province (LIP), that the basaltic magmatism resulted from lateral flow of the Tarim plume material along the margins of the Tarim craton (Pirajno et al., 2008; Qin et al., 2011; Su et al., 2011, 2012; Tang et al., 2013; Zhang et al. 2008).

The Huangshan (Huangshanxi in some literature) intrusion is a small mafic–ultramafic intrusion that hosts the second largest Ni–Cu sulfide deposit in the area (M.J. Zhang et al., 2011; Qin et al., 2003). The sulfide ore formation can be divided into a conduit stage and an in-situ differentiation stage (Y.J. Mao et al., 2014). Zhou et al. (2004) suggested that the intrusion was formed as a result of intracontinental plume-related activity, whereas M.J. Zhang et al. (2011) and Song et al. (2013) proposed that geochemical data preclude a genetic link between the Tarim LIP and the Huangshan intrusion, with Song et al. (2013) proposing that the intrusion was formed by syn-collisional magmatism induced by slab breakoff. Alternatively Branquet et al.

* Corresponding author at: State Key Laboratory of Ore Deposit Geochemistry Institute of Geochemistry, Chinese Academy of Sciences 46th Guanshui Road, Guiyang, 550002, China. Tel.: +86 0851 5895538; fax: +86 0851 5891664.
E-mail address: songxieyan@vip.gyig.ac.cn (X.-Y. Song).

http://dx.doi.org/10.1016/j.lithos.2015.04.014
0024-4937/

(2012) proposed that the Huangshan intrusions were synkinematic sheeted intrusions unrelated to rifting that formed in kilometer-scale tension gashes generated by Permian dextral shearing during post-orogenic extension. With no clear consensus as to the tectonic setting and genesis of the intrusion, we use mineral chemistry, major element oxides, trace elements and isotope data from the Huangshan intrusion to investigate its petrogenesis.

2. Geological background

The Central Asian Orogenic Belt is a complex collage of continental fragments, island arc assemblages, remnants of oceanic crust and continental margins, set between the Siberian Craton to the north and the Tarim-North China Craton to the south (Fig. 1a; Jahn et al., 2000; Jahn, 2004; Sengör et al., 1993; Windley et al., 2007; Xiao et al., 2004, 2008). The southern CAOB in northwest China consists, from north to south, of the Chinese Altai, Junggar and Tianshan terranes and the Beishan Fold Belt (Fig. 1b). The Tianshan terrane can be further divided into three tectonic units: the Northern, Central and Southern Tianshan (Fig. 1c; BGMX, 1993; Xiao et al., 2008).

The Northern Tianshan is separated from the Central Tianshan by the Aqikkuduk fault and comprises, from north to south, the Harlik island arc, the Bogda intra-arc basin, the Dananhu island arc, the Kanggur-Yamansu intra-arc basin, (Jahn et al., 2000; Ma et al., 1993; Qin et al., 2002; Xiao et al., 2004, 2008; Fig. 1c). The Harlik arc terrane consists of Ordovician metamorphosed clastic and volcaniclastic rocks, tholeiitic basalts, andesites and minor marbles. Yuan et al. (2010) proposed that a slab break-off regime, following accretion of the Harlik arc onto the Angara continent, may explain the gabbroic and A-type granitic intrusions in this area. The Bogda intra-arc basin comprises Carboniferous bimodal volcanic rocks, marine carbonate rocks and epicontinental detrital rocks, as well as Permian volcaniclastic rocks, conglomerates and sandstones. Recent studies have suggested that the Permian bimodal volcanism in the southern Bogda zone was formed in a post-collisional tectonic setting, triggered by slab break-off (Chen et al., 2011; Shu et al., 2010). Chen et al. (2013) recognized Carboniferous bimodal volcanism in the Bogda intra-arc basin and proposed that it was formed from back-arc extensional magmatism, induced by the subduction of the Junggar plate during the Late Paleozoic. The Dananhu arc is composed of Ordovician–Carboniferous tholeiitic basalt, calc-alkaline andesite and pyroclastic rocks (Li et al., 2006a; Qin et al., 2002). Several Early Permian mafic–ultramafic intrusions have been recognized in the terrane, but Ni–Cu mineralization has not yet been discovered (Li et al., 2006b). The Permian Shaerhu alkaline complex was formed as a result of oblique subduction that gave rise to strike-slip extensional faults, which controlled the emplacement of the parent magma (Q.G. Mao et al., 2014).

The Kanggur–Yamansu intra-arc basin contains Early Carboniferous submarine lavas, turbidites, pyroclastic rocks, basalt flows and andesitic tuffs and tuffaceous sandstones (BGMX, 1993; Xiao et al., 2004). The

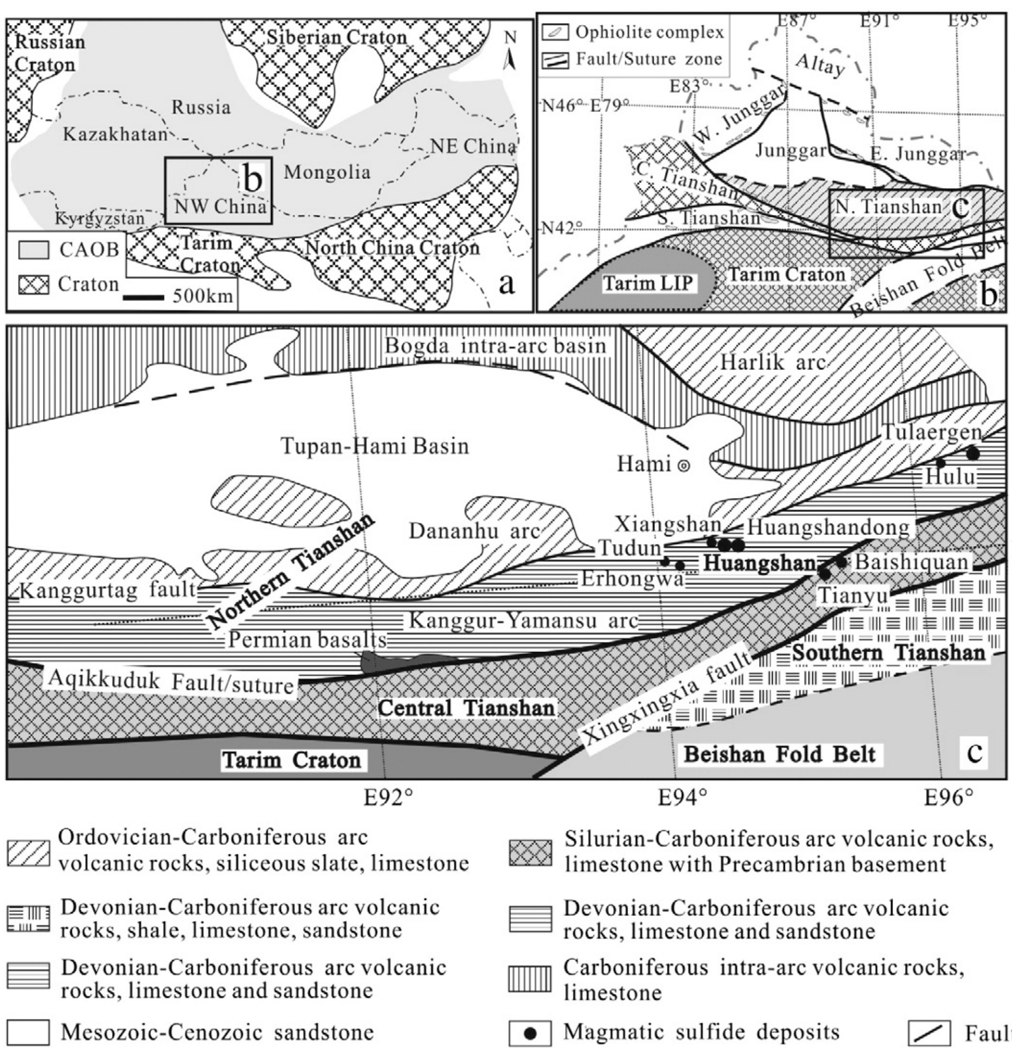

Fig. 1. (a) Schematic geological map of the Central Asian Orogenic Belt (after Jahn et al., 2000; Xiao et al., 2009); (b) tectonic blocks of northern Xinjiang (after BGMX, 1993; Song and Li, 2009; Song et al., 2013); (c) simplified geological map of Northern Tianshan (after BGMX, 1993; Song et al., 2011; Xiao et al., 2004; Zhang et al., 2013).

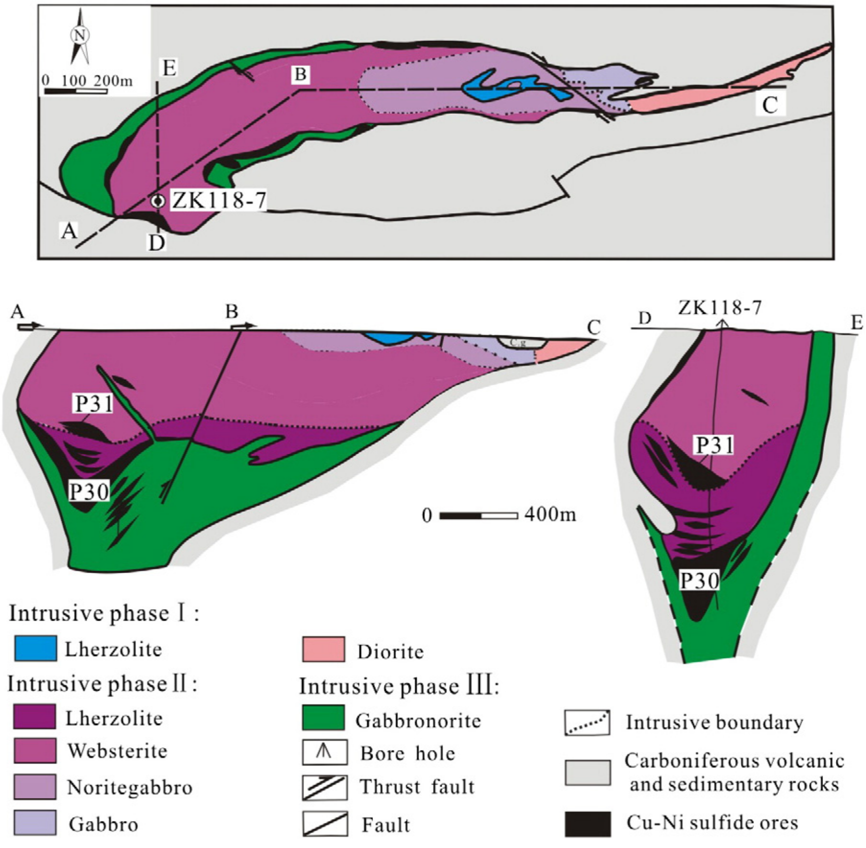

Fig. 2. Simplified geological map and cross sections of the Huangshan intrusion, showing the distribution of lithological units and sulfide ore bodies (after Li et al., 1989).

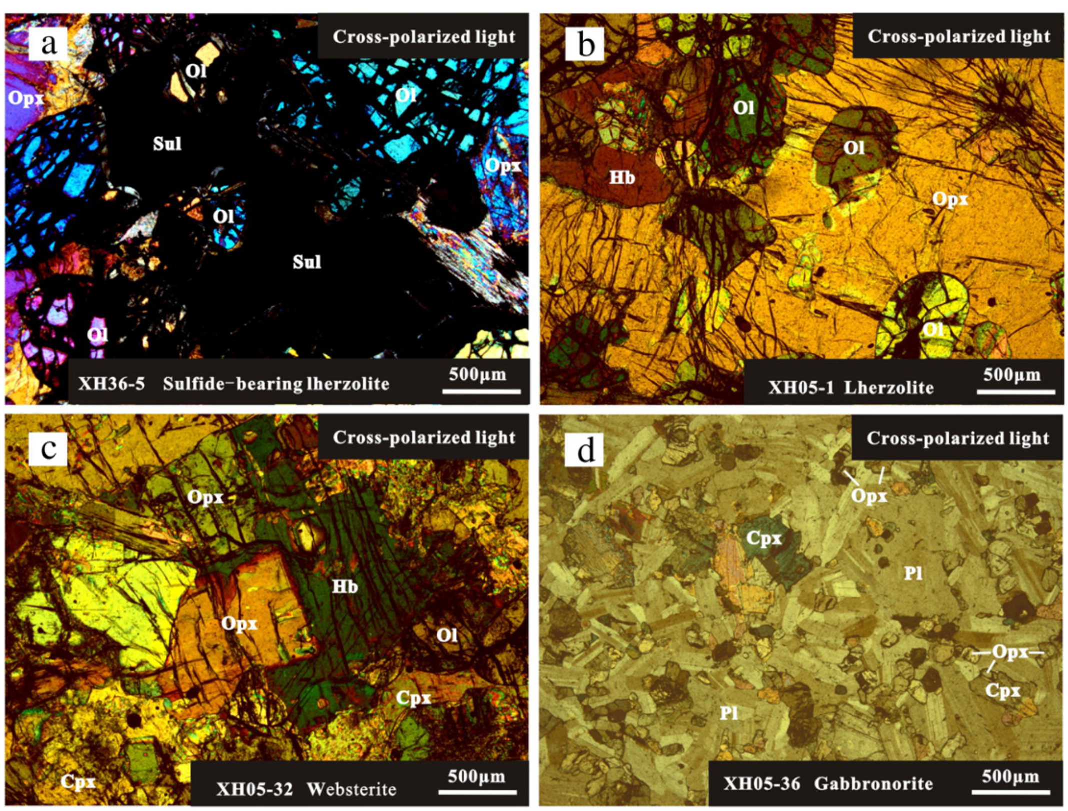

Fig. 3. Photomicrographs of the rocks from the Huangshan intrusion showing the dominant textures of sulfide-bearing lherzolite (a), olivine embedded in orthopyroxene in lherzolite (b), websterite (c), orthopyroxene and clinopyroxene in gabbronorite (d). Ol—olivine; Opx—orthopyroxene; Cpx—clinopyroxene; Pl—plagioclase; Hb—hornblende; Sul—sulfide.

Table 1
Olivine compositions of the Huangshan mafic–ultramafic intrusion.

Sample	Rock type	n	SiO_2	TiO_2	FeO	MnO	MgO	CaO	NiO	Total	Fo	Ca
			wt.%								mol%	ppm
XH09-17	Lherzolite	10	39.7	0.011	16.6	0.22	42.6	0.052	0.051	99.2	82.1	375
XH36-5		6	39.8	0.021	16.3	0.19	42.6	0.058	0.082	98.9	82.4	419
XH36-7		5	39.8	0.001	15.88	0.22	43.1	0.047	0.11	99.1	82.9	337
XH09-19	Websterite	9	40.0	0.005	17.5	0.22	42.1	0.053	0.063	99.9	81.1	382
XH09-20		5	39.4	0.019	17.5	0.23	41.7	0.047	0.054	99.0	80.9	340
XH09-22		4	39.8	0.015	17.2	0.21	42.0	0.047	0.047	99.3	81.3	340
XH09-23		6	40.0	0.018	16.3	0.21	42.6	0.074	0.063	99.2	82.4	530
XH09-25		5	40.0	0.016	16.8	0.25	42.5	0.044	0.077	99.6	81.8	315
XH09-26		8	39.9	0.015	17.1	0.22	42.2	0.063	0.037	99.5	81.5	449
XH05-6		4	39.7	0.016	23.70	0.28	35.1	0.063	0.04	99.0	72.5	450
XH05-7		5	39.3	0.020	21.51	0.41	38.4	0.051	0.09	99.9	76.3	364

geochemical compositions of the Early Carboniferous basalts and andesites are consistent with an island arc or back-arc origin (Hou et al., 2006, 2014). The Carboniferous arc-related volcano-sedimentary and plutonic rocks are crosscut by younger Permian intrusions. The Carboniferous intrusions are generally highly deformed, whereas the Permian intrusions exhibit syn-tectonic deformation related to dextral wrenching (Wartes and Carroll, 2002). The native copper bearing basalts (307-317.7 Ma) found in the western part of the Kanggur–Yamansu intra-arc basin have been interpreted to be derived from mafic magmatism generated through lithospheric delamination processes (Yuan et al., 2007; Zhang et al., 2013). Zhou et al. (2010) and Gu et al. (2006) proposed that the 320 to 250 Ma granitoids in the Northern Tianshan were formed during

Table 2
Major oxides and trace elements abundances of the Huangshan intrusion.

Rock type	Lherzolite	Websterite							Gabbronorite					
Sample	XH09-16	XH09-14	XH09-21	XH09-24	XH08-3	XH08-8	XH08-9	XH08-11	XH08-12	XH09-18	XH09-2	XH09-4	XH09-6	XH09-8
Oxides (wt.%)														
SiO_2	36.9	48.3	42.8	45.0	49.4	50.0	50.1	50.3	49.0	53.0	53.9	53.6	53.8	53.0
TiO_2	0.16	0.33	0.29	0.22	0.41	0.39	0.42	0.42	0.37	1.03	1.08	1.06	0.96	1.15
Al_2O_3	2.48	3.88	4.12	3.47	6.30	7.23	7.46	5.76	6.30	17.0	16.7	17.0	16.9	16.9
$(Fe_2O_3)_T$	15.2	11.5	8.89	10.4	9.96	7.23	7.14	8.08	9.88	7.46	7.81	7.84	7.76	7.92
MnO	0.18	0.18	0.14	0.15	0.17	0.15	0.15	0.16	0.17	0.12	0.13	0.13	0.13	0.13
MgO	32.7	25.0	24.0	26.5	22.2	16.6	16.9	19.1	22.9	6.1	6.1	6.12	6.27	6.35
CaO	2.15	3.04	6.20	5.97	10.2	14.9	15.3	14.1	10.0	8.67	8.33	8.46	8.53	8.58
Na_2O	0.040	0.200	0.010	0.040	0.62	0.60	0.54	0.54	0.54	3.45	3.44	3.4	3.41	3.38
K_2O	0.13	0.04	0.74	0.11	0.17	0.15	0.11	0.15	0.15	0.47	0.93	1.09	0.86	0.91
P_2O_5	0.035	0.020	0.035	0.034	0.069	0.044	0.050	0.066	0.056	0.14	0.15	0.13	0.14	0.15
Cr_2O_3	0.29	0.33	0.27	0.29						0.020	0.020	0.020	0.020	0.020
LOI	9.51	7.44	11.1	7.57	0.58	2.03	1.64	1.15	0.39	1.79	0.27	0.93	0.96	1.08
Total	99.8	100	98.5	99.7	100	99.2	99.8	99.8	99.7	99.2	98.9	99.8	99.7	99.6
Trace element (ppm)														
Sc	8.67	24.5	31.1	27.5	41.0	58.6	59.9	57.5	39.8	23.9	26.2	26.5	26.8	25.9
Cr	2110	2460	2320	2380	1930	754	926	1530	2170	171	185	179	191	188
Co	168	178	91.3	101	80.0	51.3	49.4	63.6	80.9	29.3	31.0	31.8	32.0	32.0
Ni	1360	2650	362	412	256	144	109	179	248	25.3	21.6	25.3	54.6	40.8
Cu	747	1350	92.0	73.0	56.8	45.8	40.1	51.8	45.3	31.7	19.3	22.3	56.7	35.7
Rb	2.34	0.42	24.6	2.30	3.66	3.65	4.75	4.85	3.67	8.07	21.2	25.8	17.9	19.1
Sr	37.4	19.8	147	81.1	100	134	135	72.9	107	419	407	412	419	419
Y	3.49	5.86	7.37	6.87	9.16	11.6	11.6	11.4	9.20	20.9	22.4	21.4	20.5	20.8
Zr	13.7	25.2	25.7	22.1	33.2	27.5	25.0	30.3	30.7	85.2	112	108	86.9	84.2
Nb	0.54	0.76	0.63	0.53	0.58	0.26	0.23	0.39	0.57	2.94	3.40	3.32	2.78	3.34
Ba	30.8	6.79	126	26.8	38.9	30.0	31.8	37.7	39.3	113	226	234	213	218
La	1.23	2.02	2.51	2.20	2.07	1.28	1.29	1.68	1.81	8.13	9.44	8.94	8.28	8.53
Ce	2.86	4.65	5.78	5.14	5.27	3.79	3.82	4.58	4.86	18.8	21.9	20.6	19.1	19.5
Pr	0.41	0.70	0.84	0.74	0.86	0.68	0.70	0.80	0.81	2.56	3.06	2.86	2.70	2.67
Nd	2.07	2.87	3.81	3.44	4.21	3.84	3.84	4.23	4.18	11.9	13.8	12.7	12.1	12.6
Sm	0.50	0.836	1.07	0.98	1.30	1.42	1.48	1.51	1.34	3.04	3.28	3.42	3.31	3.17
Eu	0.20	0.26	0.29	0.39	0.43	0.48	0.49	0.46	0.42	1.22	1.30	1.31	1.24	1.25
Gd	0.59	1.00	1.35	1.22	1.37	1.66	1.64	1.70	1.32	3.55	3.86	3.50	3.52	3.56
Tb	0.10	0.15	0.24	0.21	0.27	0.34	0.35	0.33	0.28	0.59	0.66	0.60	0.62	0.63
Dy	0.58	0.92	1.41	1.21	1.67	2.16	2.14	2.10	1.63	3.51	4.00	3.87	3.65	3.61
Ho	0.14	0.23	0.30	0.29	0.39	0.47	0.50	0.46	0.37	0.74	0.89	0.84	0.80	0.79
Er	0.38	0.72	0.84	0.77	1.00	1.26	1.22	1.20	0.91	2.05	2.43	2.25	2.27	2.25
Tm	0.046	0.10	0.12	0.12	0.14	0.18	0.18	0.17	0.13	0.31	0.33	0.31	0.31	0.32
Yb	0.33	0.72	0.73	0.73	0.98	1.11	1.04	1.05	0.84	1.95	2.19	2.18	2.05	2.06
Lu	0.052	0.11	0.10	0.10	0.13	0.16	0.14	0.14	0.13	0.30	0.30	0.31	0.29	0.30
Hf	0.36	0.69	0.67	0.62	0.99	0.85	0.89	0.96	0.93	2.15	2.82	2.84	2.22	2.17
Ta	0.047	0.057	0.045	0.063	0.069	0.027	0.031	0.047	0.056	0.22	0.25	0.25	0.22	0.26
Th	0.31	0.59	0.48	0.38	0.36	0.16	0.14	0.32	0.32	1.41	1.94	1.96	1.54	1.42
U	0.14	0.20	0.21	0.17	0.14	0.16	0.06	0.14	0.12	0.54	0.78	0.78	0.62	0.53
Pb	0	1.01	2.71	2.51	1.21	0.58	0.79	1.03	0.76	5.14	6.39	6.23	6.03	5.86

the post-collision period. Around 290 to 270 Ma, the Jiaoluotage ductile compressional zone was formed as a result of N–S-oriented horizontal coaxial compression, caused by the collision between the Tarim paleo-ocean plate and the middle Tianshan arc–Jiaoluotage basin–Jungar plate system (Xu et al., 2003). The main east–west ductile shear zones were dextral and coeval with greenschist retrograde metamorphism that decreases eastward (Laurent-Charvet et al., 2003; Shu et al., 1999). In the early stage of ductile deformation, the shear zone was characterized by nappe shearing, starting after 300 Ma and lasting to at least 284 Ma, as a result of the latest Paleozoic continental collision (Chen et al., 2005). The Kanggur gold deposit was formed during the transition between compression and extension during this collision (Zhang et al., 2003). Branquet et al. (2012) proposed that the Huangshan mafic–ultramafic rocks were synchronous with Early Permian regional strike-slip deformation and the ductile shear deformation and associated gold mineralisation in the Early Permian occurred in a syn-collision setting.

3. Petrography and mineralization of the Huangshan intrusion

The Huangshan intrusion is located at the northern margin of the Kanggur–Yamansu intra-arc basin (Fig. 2c). Zhou et al. (2004) reported a SHRIMP zircon U–Pb age of 269 ± 2 Ma for the diorite, whereas the gabbros yielded crystallization ages of 284.5 ± 2.5 Ma and 283.8 ± 3.4 Ma by zircon U–Pb LA-ICP-MS and SIMS (Gu et al., 2006; Qin et al., 2011). The gabbros are thought to best represent the age of crystallization with the diorite having been emplaced later.

The intrusion is approximately 2.5 km long and 50–400 m wide with an area of 3.8 × 0.8 m^2 (Fig. 2). It intruded the siltstone, limestone and spilite of the Late Carboniferous Gandun formation (Li et al., 1989). Magma emplacement resulted in contact metamorphism that formed an aureole between 5 and 50 m wide. The limestones have been metamorphosed to garnet–diopside–wollastonite marble and are present as xenoliths in the intrusion (Wang et al., 1987).

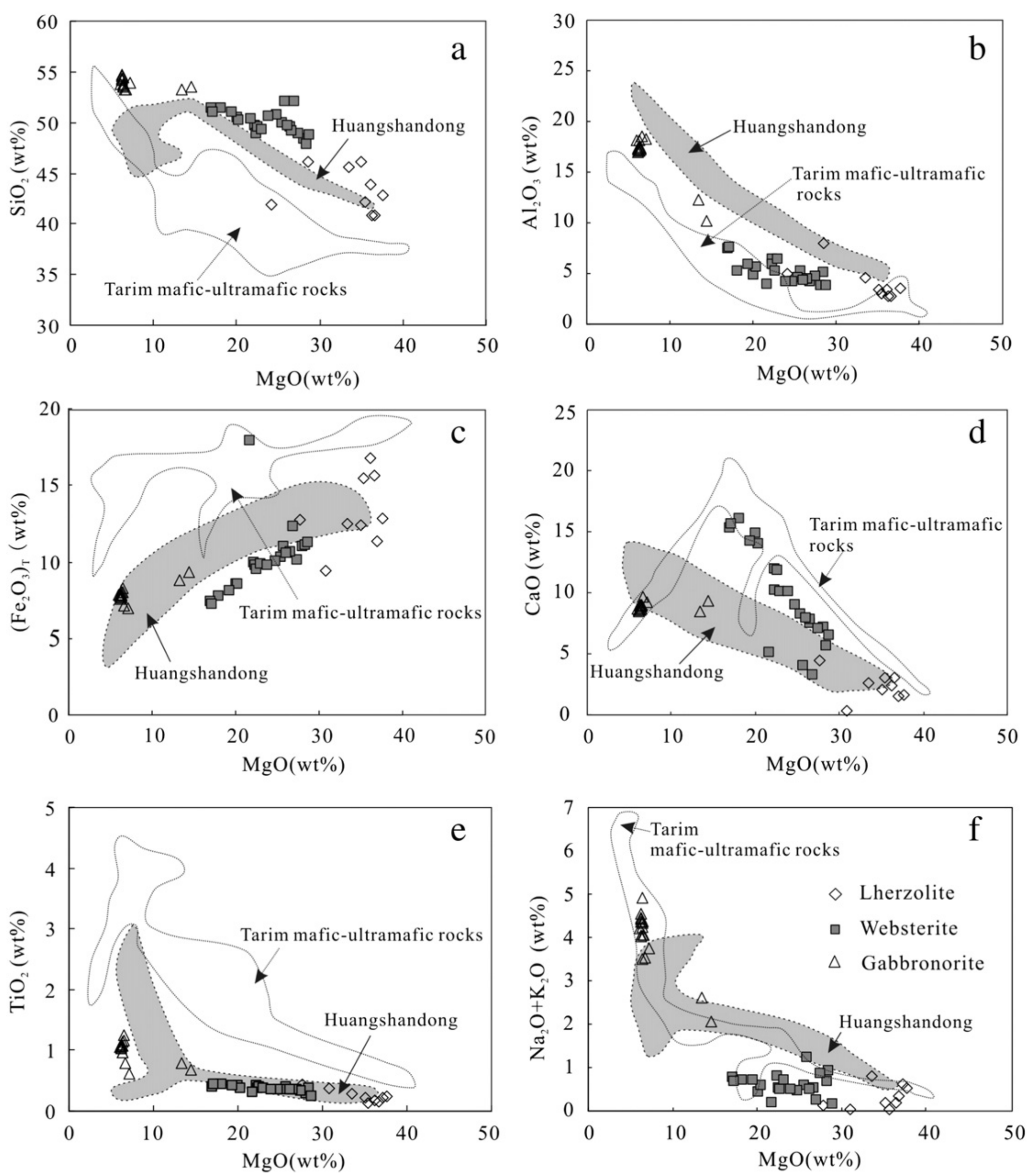

Fig. 4. Harker diagrams of the Huangshan intrusion. Additional whole-rock data for the Huangshan and Huangshandong intrusions are from Deng et al. (2011a,b, 2014) and Song et al. (2013).

The Huangshan intrusion is comprised of the eastern peridotite, the basal gabbronorite and the middle mafic–ultramafic unit with the following rock types (from the base upwards): lherzolite, websterite, norite gabbro, gabbro and diorite. The eastern peridotite is crosscut by the norite gabbro of the middle unit, whereas the basal gabbronorite crosscuts the lherzolite of the middle unit (Fig. 2; Li et al., 1989). The contacts between the rocks in the middle suite are typically gradational. Mineral assemblages and sharp contacts between the three intrusive phases of the Huangshan intrusion suggest that there were three magmatic stages. The first stage formed the peridotite in the eastern part of the intrusion, the second stage formed the middle mafic–ultramafic unit which comprises the main part of the intrusion, whereas the gabbronorite represents the last intrusive phase (Li et al., 1989; Zhou et al., 2004).

The eastern peridotite comprises <2% of the intrusion and is suspended in the gabbronorite of the middle unit. It contains 60–80% olivine, 20–25% pyroxene, 10–15% plagioclase, 10–15% hornblende and 1–2% phlogopite (Wang et al., 1987). The lherzolite comprises 50–70% olivine, 5–25% orthopyroxene, 0–15% clinopyroxene, 5–15% hornblende, and minor phlogopite (Fig. 3a, b). The olivine crystals are sub-rounded and enclosed in large orthopyroxene, clinopyroxene, plagioclase, and hornblende. Some orthopyroxenes are enclosed in clinopyroxene and hornblende oikocrysts. The sulfides are commonly interstitial, but small, rounded sulfide inclusions are also enclosed in some olivine crystals. Trace Cr-spinel is present as small inclusions in silicate minerals.

The websterite is composed of 20–35% olivine, 15–50% orthopyroxene, 10–25% clinopyroxene, 5–15% hornblende, 2–5% sulfide and 0–3% plagioclase (Fig. 3c). The olivine crystals are enclosed in poikilitic orthopyroxene, clinopyroxene and hornblende. Some olivine crystals contain clinopyroxene (Fig. 3d) whereas most orthopyroxenes are intergrown with clinopyroxene and a few are surrounded by clinopyroxene and hornblende. Some granular clinopyroxene and orthopyroxene crystals have reaction coronae of hornblende (Fig. 3e).

The gabbronorite consists of 50–55% plagioclase, 15–20% orthopyroxene, 10–15% clinopyroxene, 5–15% hornblende, and 1–3% phlogopite plus minor sulfide (1–3%). Orthopyroxene is either intergrown with clinopyroxene or enclosed in plagioclase (Fig. 3d).

The Ni–Cu sulfide orebodies are dominantly located at the base of the websterite and lherzolite horizons, with rare small sulfide veins occuring in the underlying gabbronorite (Fig. 2). The Huangshan deposit contains 0.32 Mt Ni and 0.18 Mt Cu with an average grade of 0.49 wt.% Ni and 0.31 wt.% Cu (Qin et al., 2003). Disseminated sulfides comprise the dominant ores of the Huangshan Ni–Cu deposit with only rare massive sulfide ores. The largest ore body, P30, occurs in the lowermost lherzolite and contains about 85% of the total tonnage in the Huangshan deposit, whereas the second largest ore body, P31, is located in the lowermost of the websterite layers and contains about 10% of the total tonnage (Li et al., 1989). The ore minerals include pyrrhotite, pentlandite and chalcopyrite with lesser bornite, magnetite and chromite.

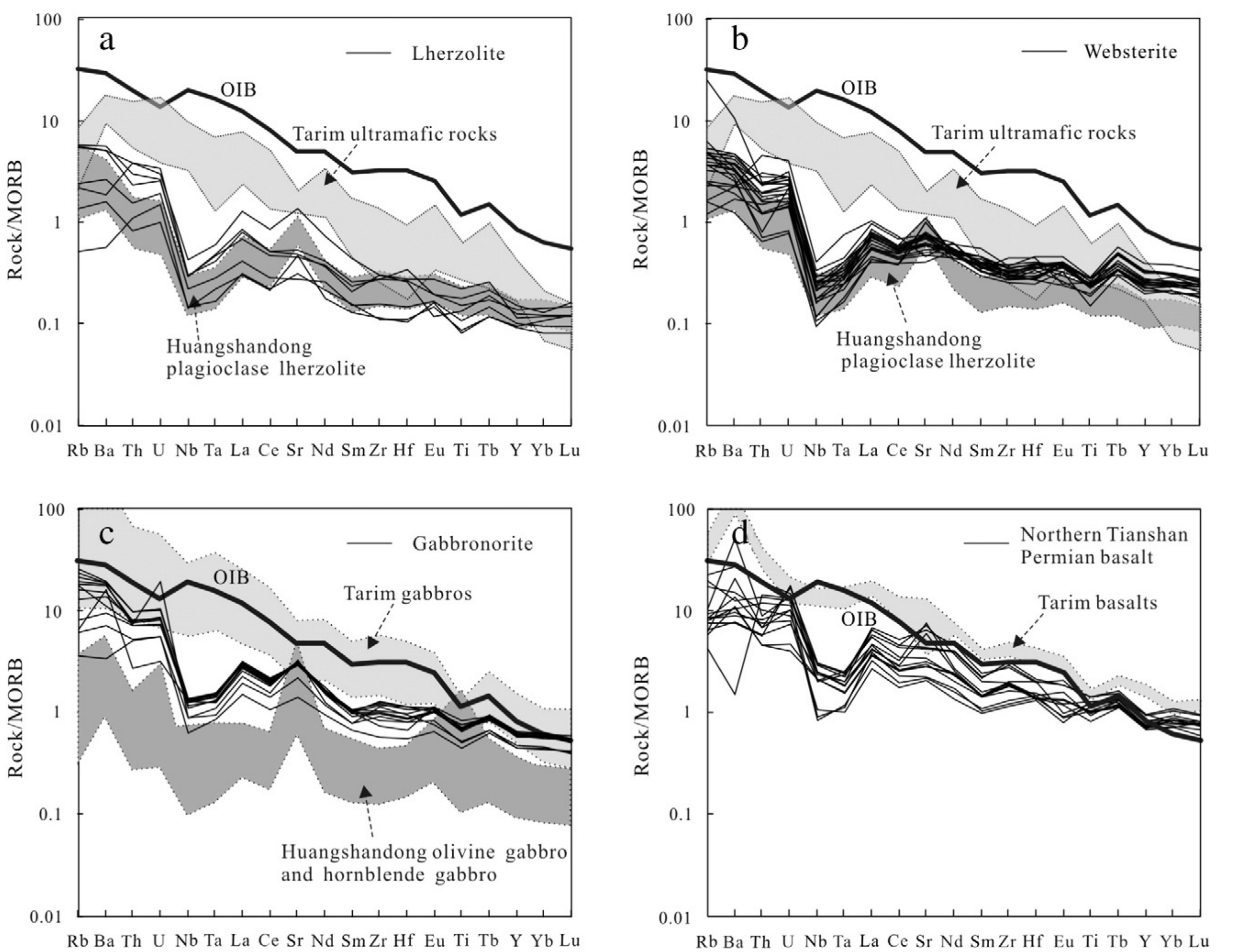

Fig. 5. N-MORB normalized trace element spider diagrams of the Huangshan intrusion. Additional data for the Huangshan and Huangshandong intrusions are from Deng et al. (2011a,b, 2014) and Song et al. (2013). The whole-rock data for the basalts in Northern Tianshan are from Zhou et al. (2006), Chen et al. (2011) and Zhang et al. (2013). The data for the mafic–ultramafic rocks of the Tarim LIP are from Jiang et al. (2004a,b), Zhang et al. (2008) and Zhou et al. (2009). The data for N-MORB and OIB are taken from Pearce (1982) and Sun and McDonough (1989), respectively.

4. Analytical methods

The thirty-three samples used in this study were from weakly altered outcrops, underground mine workings and drill core (ZK118-7), including sulfide-bearing lherzolite, lherzolite, websterite and gabbronorite. Analyses of major and trace elements were conducted at the State Key Laboratory of Ore Deposit Geochemistry (SKLODG) in the Institute of Geochemistry, Chinese Academy of Science. Whole-rock abundances of major oxides were analyzed with a PANalytical Axios-advance X-ray fluorescence spectrometer (XRF) on fused glass pellets with analytical uncertainties ranging from 1 to 3%. Analytical results of standard materials and replicate analyses are presented in Appendix 1. Trace elements were determined by Inductively Coupled Plasma Mass Spectrometry (ICP-MS) using the procedure described by Qi et al. (2000). Reference standards, BHVO-2, GBPG-1 and replicate analyses, were used to monitor the trace element analyses (Appendix 2). The analytical uncertainty is better than 5%.

Olivines from the Huangshan intrusive rocks were analyzed by wavelength-dispersive X-ray analysis using an EPMA-1600 electron microprobe at the SKLODG. The accelerating voltage was 15 kV, the beam current was 20 nA, and the counting time was set at 10 s. Standard Program International (SPI) mineral standards (USA) were used for calibration. Replicate analytical results of natural mineral standards are presented in Appendix 3.

For radiogenic isotope analysis approximately 120 mg of powdered sample was placed in Teflon beakers with a HF + HNO_3 mixture and then heated on a hotplate at about 120 °C for one week. Strontium and Nd were then separated and purified by conventional cation-exchange techniques. The isotopic compositions of purified Sr and Nd solutions were measured on a TRITON thermal ionization magnetic sector mass spectrometer (TIMS) at the SKLODG using the procedure described by Yang et al. (2010). Mass fractionation corrections for Sr and Nd isotopic ratios were based on values of $^{86}Sr/^{88}Sr = 0.1194$ and $^{146}Nd/^{144}Nd = 0.7219$. Analyses of the NBS-987 Sr standard yielded an $^{86}Sr/^{88}Sr$ ratio of 0.710255 ± 7 (n = 40), whereas analyses of the JNdi-1 Nd standard yielded a $^{146}Nd/^{144}Nd$ ratio of 0.512096 ± 5 (n = 40). Uncertainties in Rb–Sr and Sm–Nd ratios are less than ±2% and ±0.5% (relative), respectively.

5. Geochemistry of the Huangshan intrusion

Olivine grains were analyzed from the lherzolite and websterite units of the Huangshan intrusion (Table 1). Forsterite (Fo) contents in the olivines of the lherzolite range from 82.1 to 82.9, whereas those of the websterite are 72.5–82.4. The olivine crystals in all these samples have low Ca content (<1000 ppm; Table 1). Representative major element contents of the Huangshan rocks are listed in Table 2 and have been recalculated to 100% on a volatile–free basis for use in this paper. The lherzolites have higher MgO, $(Fe_2O_3)_T$ and lower Al_2O_3, CaO, TiO_2 and alkali elements than the websterites (Table 2; Fig. 4). The gabbronorites have lower MgO and $(Fe_2O_3)_T$ and higher SiO_2, Al_2O_3, CaO, (K_2O + Na_2O) and TiO_2 contents than the websterites.

On normal Mid-Ocean Ridge Basalts (N-MORB) normalized trace element diagrams the Huangshan intrusive rocks are enriched in large ion lithophile elements (Rb, Th, U, and La) relative to the high field strength elements and display strong negative Nb–Ta–Ti anomalies (Fig. 5). The Rb–Sr and Sm–Nd isotopic data for the Huangshan intrusion are provided in Table 3. Strontium and Nd isotope data for the intrusion are calculated to have an initial age of 283.8 Ma from Qin et al. (2011). The samples have low initial $^{87}Sr/^{86}Sr$ ratios (0.703046–0.703877) and high $\varepsilon Nd_{(t)}$ (5.14–7.24; Fig. 6).

6. Discussion

Compared with the Tarim mafic–ultramafic rocks, the Huangshan and Huangshandong rocks have higher SiO_2, Al_2O_3 and lower $(Fe_2O_3)_T$, CaO, and TiO_2 contents (Fig. 4). The trace element patterns of the Huangshan and Huangshandong intrusions are similar to those of the Permian basalt in the Northern Tianshan, but are distinct from the modern OIB and the Tarim plume-related mafic–ultramafic rocks (Fig. 5). The Sr–Nd isotopic compositions of the Northern Tianshan intrusions lie between the field of asthenospheric and lithospheric mantle sources with most basalts of the Northern Tianshan plotting in the field of lithospheric mantle. The majority of the mafic–ultramafic rocks in the Northern Tianshan lie outside the field for the Tarim plume-related rocks (Fig. 6). These geochemical differences are not consistent with a genetic relationship between the mafic–ultramafic rocks in Northern Tianshan and the Tarim plume. The Huangshan intrusive rocks have higher SiO_2 and CaO contents, but lower Al_2O_3, $(Fe_2O_3)_T$ and K_2O + Na_2O than the Huangshandong rocks (Fig. 4). Compared with the Huangshandong intrusion, the Huangshan rocks have higher $^{87}Sr/^{86}Sr_{(t)}$ (0.702921–0.703710) and lower $\varepsilon Nd_{(t)}$ (5.84–9.92) (Deng et al., 2011a,b; Song et al., 2013; Zhou et al., 2004). This suggests that the Huangshan and Huangshandong rocks were derived from different mantle sources. Because different tectonic settings will have unique isotopic signatures, identifying the mantle source of the Huangshan rocks can be used to constrain the tectonic setting. In the following discussion, we compare geochemical compositions of the mafic–ultramafic

Table 3
Sr, Nd isotopes for the rocks of the Huangshan intrusion.

Rock type	Websterite		Gabbronorite	
Sample	XH08-5	XH08-7	XH05-30	XH08-1
Rb (ppm)	1.59	6.09	5.24	13.0
Sr (ppm)	54.3	78.3	394	405
$^{87}Rb/^{86}Sr$	0.08	0.2249	0.0384	0.0928
$^{87}Sr/^{86}Sr$	0.703989	0.704611	0.703626	0.703973
2σ	3	8	8	7
$(^{87}Sr/^{86}Sr)_0$	0.703665	0.703750	0.703479	0.703618
Sm (ppm)	1.51	1.78	1.48	3.34
Nd (ppm)	4.07	4.84	6.66	12.5
$^{147}Sm/^{144}Nd$	0.22415	0.2222	0.13433	0.1614
$^{143}Nd/^{144}Nd$	0.512981	0.512985	0.512899	0.512890
2σ	4	4	1	2
$(^{143}Nd/^{144}Nd)_0$	0.512586	0.512594	0.512662	0.512606
εNd(t)	5.75	5.90	7.24	6.13

Note: The initial isotopic ratios were calculated at 284.5 Ma.

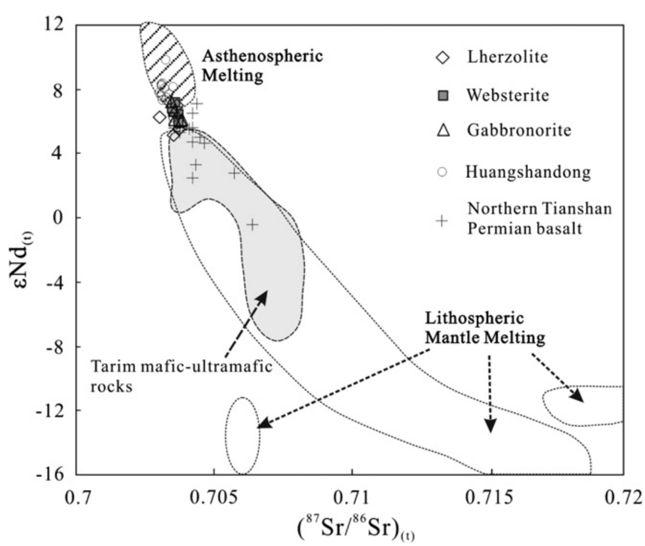

Fig. 6. Isotopic data for the Huangshan intrusion and mantle melts (modified after Davies and von Blanckenburg, 1995). Additional data for the Huangshan and Huangshandong intrusions are from Deng et al. (2011a,b) and Song et al. (2013). The basalts in Northern Tianshan are from Zhang et al. (2013). The mafic–ultramafic rocks of the Tarim LIP are from Zhang et al. (2008) and Zhou et al. (2009).

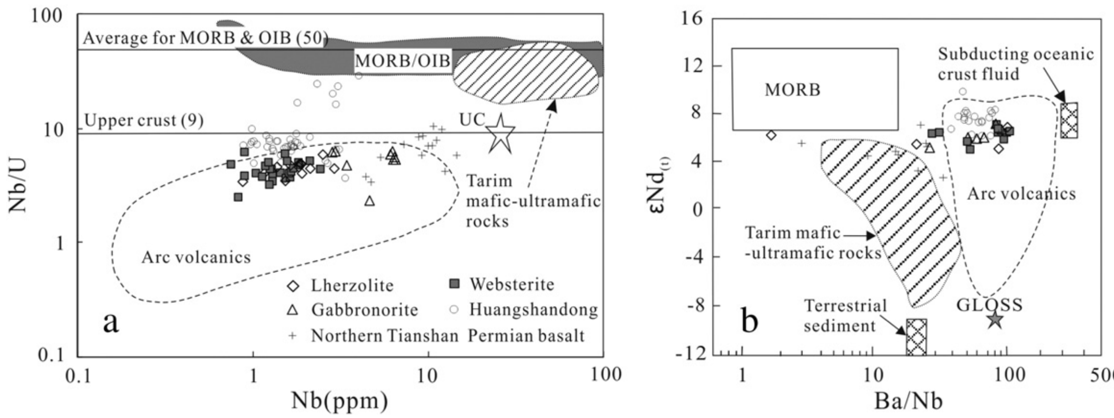

Fig. 7. Plots of (a) Nb vs. Nb/U (after Chung et al., 2001), (b) Ba/Nb vs. $\varepsilon Nd_{(t)}$ for the Huangshan intrusive rocks (after Li, 1995). Additional data for the Huangshan and Huangshandong intrusions are from Deng et al. (2011a,b, 2014) and Song et al. (2013). Data for the mafic–ultramafic rocks of the Tarim LIP are from Zhang et al. (2008) and Zhou et al. (2009). Data for oceanic island arcs are from Elliott et al. (1997), Turner et al. (1997), Pearce et al. (1995), Marini et al. (2005), Ellam et al. (1989), and Turner and Foden (2001). GLOSS data are from Plank and Langmuir (1998).

intrusions and basalts in the Northern Tianshan at different ages to identify the mantle evolution in this area and to illuminate the tectonic setting and genesis of these mafic–ultramafic rocks.

6.1. Nature of the mantle source

The similar bulk solid/melt partition coefficient of Nb and U (Hofmann, 1988; Sun and McDonough, 1989) means that they will not be significantly fractionated during magma crystallization processes, and consequently the Nb/U ratios of the rocks will reflect the ratios in the mantle source. Oceanic basalts are characterized by a nearly constant Nb/U ratio of ~50, bulk silicate Earth ~32 (McDonough and Sun, 1995) and continental upper crust ~9 (Rudnick and Fountain, 1995), whereas typical arc volcanic rocks are characterized by significantly lower Nb/U ratios (0.3–9.0; Chung et al., 2001), because the metasomatized mantle sources in a subduction setting are enriched in large ion lithophile elements and depleted in high field strength elements (Fig. 7a; Hofmann et al., 1986). If rocks are formed by contamination of the mantle end-member by continental crust, the ratios of trace elements should be intermediate between the two end-members. All the Huangshan rocks and most of the Huangshandong intrusive rocks have lower Nb/U ratios than those of OIB, MORB and continental upper crust but are similar to arc volcanic rocks (Fig. 7a). This suggest that the Nb/U ratios of the Huangshan rocks and most of the Huangshandong rocks cannot be the result of contamination of the mantle end-member by crust, but rather they indicate that the primary magma of these rocks was derived from a metasomatized mantle source. In contrast, some Huangshandong samples plot in the field of MORB, suggesting the parent magma of these samples was derived from asthenospheric mantle (Fig. 7).

Several studies have proposed that the mantle source of island-arc basalts have three primary end-member components, namely MORB-type depleted mantle, hydrous fluid released from subducted oceanic crust and subducted sediments derived from the continental crust (Li, 1995; Pearce and Peate, 1995). As shown in Fig. 7b, the intrusive rocks from the Huangshan and Huangshandong intrusions lie between the fields for MORB, subducted oceanic crust and global subducting sediment (GLOSS) and within the arc volcanic field, suggesting that both depleted and metasomatized mantle was involved in the formation of the Huangshan and Huangshandong intrusions.

$\varepsilon Nd_{(t)}$ and $(^{87}Sr/^{86}Sr)_{(t)}$ values compiled from the region do not show a correlation with SiO_2 and La/Sm in the mafic–ultramafic rocks of the Northern Tianshan (not shown), suggesting that the radiogenic isotopes have not been significantly modified by crustal contamination. The $\varepsilon Nd_{(t)}$ values increase from 2.5 to 7.1 in the 307 Ma Northern Tianshan basalts to 5.8 to 9.9 in the 274 Ma Huangshandong rocks, whereas $(^{87}Sr/^{86}Sr)_{(t)}$ ratios decrease from 0.70358–0.70580 in the Northern Tianshan basalts to 0.70292–0.70371 in the Huangshandong rocks (Fig. 8a), whereas, the $\varepsilon Nd_{(t)}$ values of the mafic–ultramafic rocks in the Northern Tianshan increase with age (Fig. 8b). The

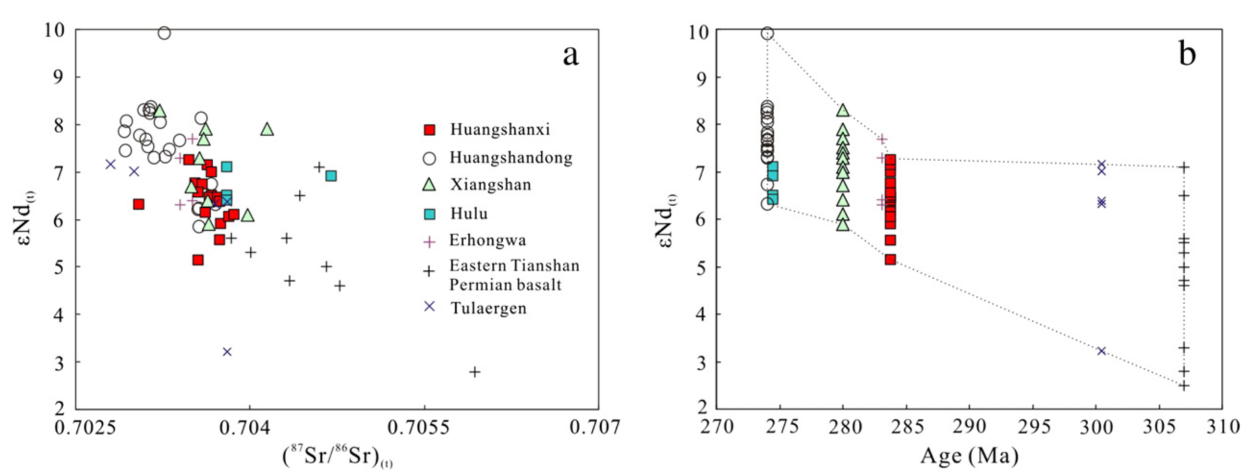

Fig. 8. Correlation diagrams of (a) $(^{87}Sr/^{86}Sr)_{(t)}$ vs. $\varepsilon Nd_{(t)}$ (b) $\varepsilon Nd_{(t)}$ vs. U–Pb ages for mafic–ultramafic rocks of the Northern Tianshan. Data for the Huangshan and Huangshandong intrusions are from Deng et al. (2011a,b) and Song et al. (2013). Isotopic data of the Xiangshan, Hulu, Erhongwa, Tulaergen intrusions and Permian basalts are from Tang et al. (2013), Xia et al. (2008), Sun et al. (2013a), Jiao et al. (2012), and Zhang et al. (2013) respectively.

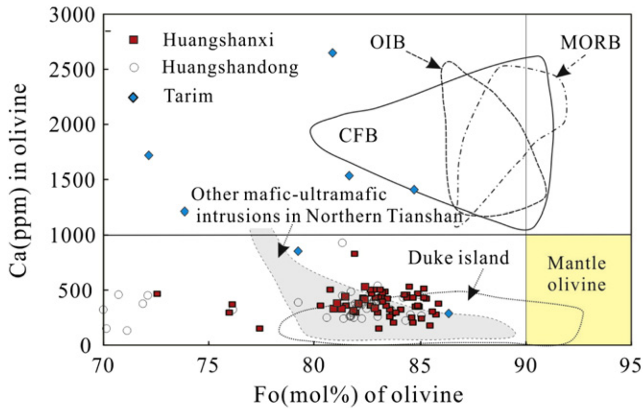

Fig. 9. Plot of Ca versus Fo contents in olivine (after Li et al., 2012). Some olivine compositions for the Huangshanxi intrusive rocks are from Mao (2014). Olivine composition for the Huangshandong intrusive rocks and the Tarim ultramafic rocks are from Deng et al. (2012) and Jiang et al. (2004a,b). Olivine compositions for the other mafic–ultramafic intrusions in northern Tianshan are from Sun et al. (2013a), Xia et al. (2008) and Mao (2014).

magma composition and mantle source characteristics of the mafic–ultramafic rocks in Northern Tianshan imply that they were produced by interaction between depleted asthenospheric melts and metasomatized lithospheric mantle. Because asthenospheric mantle has higher $\varepsilon Nd_{(t)}$ and lower $(^{87}Sr/^{86}Sr)_{(t)}$ ratios than lithospheric mantle, the variations in the radiogenic isotopes of the mafic–ultramafic rocks in the Northern Tianshan suggest that there was greater involvement of upwelling asthenospheric mantle in the younger rocks of the Northern Tianshan.

6.2. Tectonic implications

The mafic–ultramafic intrusions and A-type granites in the Northern Tianshan and adjacent tectonic units are broadly coeval (Han et al., 2004; San et al. 2010; Song et al., 2013) and overlap with the Permian Tarim mafic rocks (270–290 Ma; Chen et al., 2010; Yu et al., 2011; Zhang et al., 2008, 2012). The Permian mafic–ultramafic intrusions in the Northern Tianshan have been interpreted to be the product of the Tarim mantle plume (Mao et al., 2006; Pirajno et al. 2008; Qin et al. 2011; Su et al. 2011; Tang et al., 2013).

Because the Ca contents of olivine formed in different tectonic settings are distinct, they can be used to identify the source of the host rocks (Kamenetsky et al., 2006; Li et al., 2012). Olivine crystals from subduction-related ultramafic and mantle rocks typically have low Ca contents (<1000 ppm), whereas primitive olivine from komatiites, continental flood basalts, MORB and ocean island basalts have higher Ca contents (>1000 ppm; Fig. 9). The Ca contents of olivine from the Huangshan and Huangshandong intrusions are less than 1000 ppm, significantly lower than those of the Tarim ultramafic rocks and OIB but similar to subduction-related intrusions from Duke Island (Li et al., 2012; Thakurta et al., 2008). Studies have suggested that the variation of Ca in olivine is dependent not only on the forsterite content of the olivine but to a large extent on the amount of alumina, alkali and ferrous iron present in the coexisting melt (Jurewicz and Watson, 1988; Libourel, 1999). The similar forsterite contents of olivines from the Huangshan and Huangshandong intrusions and the Tarim ultramafic rocks means that this effect can be discounted. Compared to basalts in the Northern Tianshan, basalts from the Tarim Large Igneous Province (TLIP) have higher K_2O and $(Fe_2O_3)_T$ contents but similar CaO and Al_2O_3 (Fig. 10). This suggests that the difference in Ca contents between olivines from the Northern Tianshan and TLIP results from variable K_2O and $(Fe_2O_3)_T$ contents in the coexisting melt.

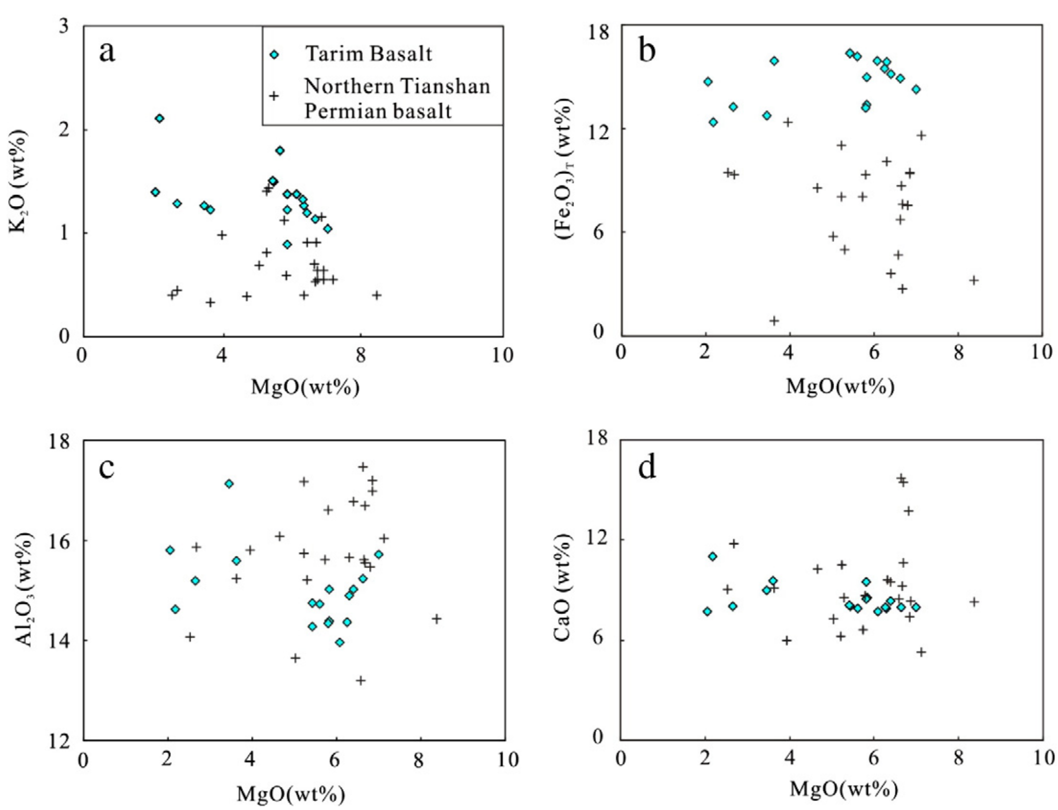

Fig. 10. Binary plots of MgO vs. K_2O (a), $(Fe_2O_3)_T$ (b), Al_2O_3 (c) and CaO (d) for the basalts of the Northern Tianshan and Tarim. Northern Tianshan basalt data are from Zhou et al. (2006), Chen et al. (2011) and Zhang et al. (2013). Tarim large igneous province data are from Zhou et al. (2009).

The mafic–ultramafic rocks in the Northern Tianshan are characterized by lower incompatible elements contents, higher εNd(t) and more depleted Nb and Ta than both the Tarim mafic–ultramafic rocks and OIB. The Huangshan and Huangshandong intrusions have Nb contents and Nb/U ratios similar to those of arc volcanic rocks (Fig. 7a). On a plot of $\varepsilon Nd_{(t)}$ versus Ba/Nb, the Huangshan and Huangshandong samples lie in the field of arc volcanic rocks and are distinct from the Tarim mafic–ultramafic rocks implying a distinct mantle source (Fig. 7b). Zhang et al. (2006) and Xiao et al. (2008) have argued that the lithospheric mantle in the Northern Tianshan was modified by subduction in the Carboniferous, but this metasomatized lithospheric mantle would have been too cold to undergo melting in the Permian (Niu, 2005; Wilson, 1989). Others have argued that the parental magmas of the mafic–ultramafic intrusions in the Northern Tianshan were derived from high degrees of melting of lithospheric mantle associated with the higher temperatures of a mantle plume head (Qin et al., 2011; Su et al., 2011, 2012; Zhou et al., 2009). The geochemical characteristics of mafic–ultramafic rocks in Northern Tianshan imply that they were produced by the interaction of metasomatized lithospheric mantle and depleted asthenospheric melts consistent with partial melting of metasomatized lithospheric mantle triggered by upwelling depleted asthenospheric melts rather than a mantle plume. Underplating of the upwelling asthenosphere would have provided sufficient heat to melt the Carboniferous residual metasomatized mantle.

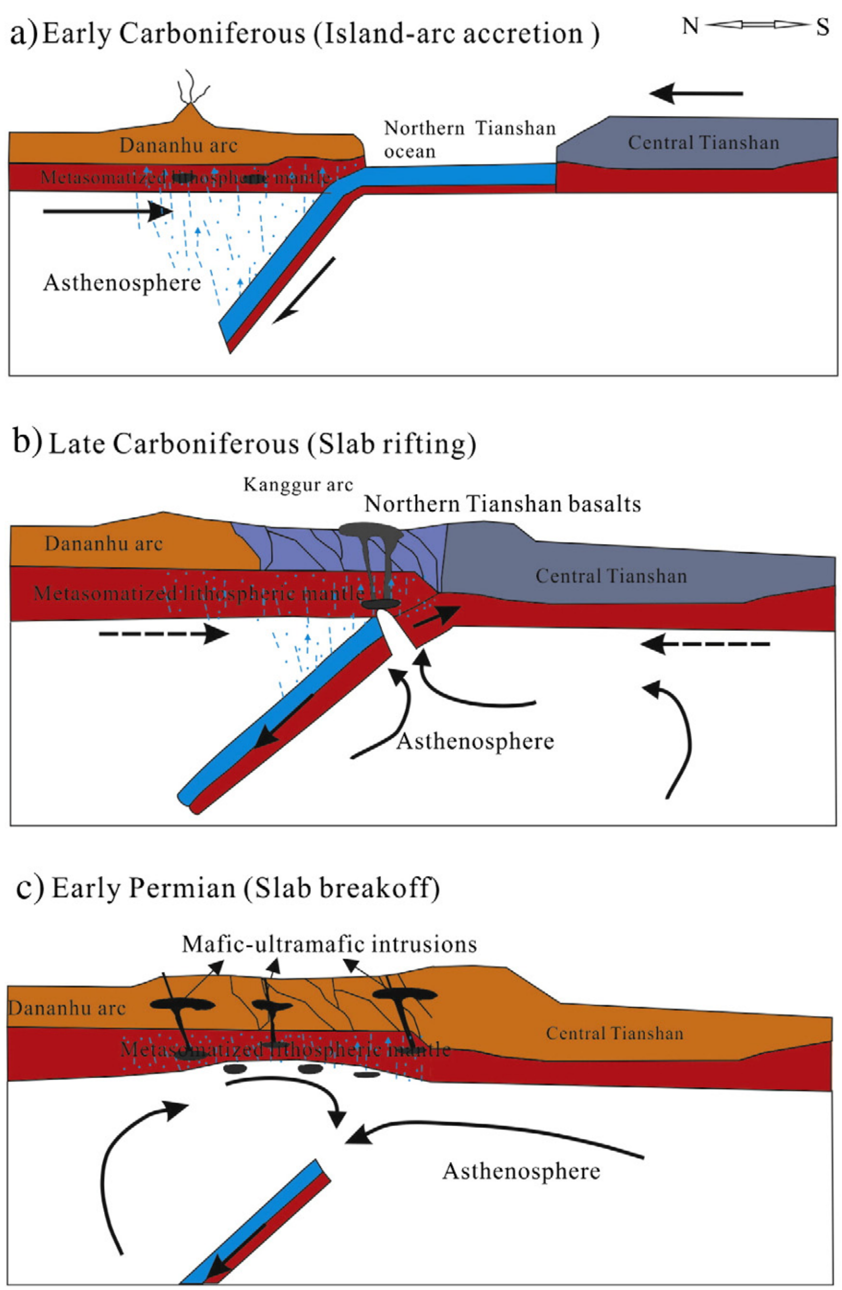

Fig. 11. Schematic diagram showing the Late Paleozoic tectonic evolution of the Eastern Tianshan (after Davies and von Blanckenburg, 1995; Song et al., 2013; Yuan et al., 2010). (a) Northern Tianshan oceanic slab subducted northward during the period between Late Ordovician to Late Carboniferous; (b) the oceanic lithosphere separates from the continental lithosphere due to negative buoyancy, resulting in upwelling of asthenospheric mantle through the gap after the closure of the Northern Tianshan Ocean; (c) detachment of the oceanic lithosphere induces an extensional regime and causes partial melting in the asthenosphere and overriding metasomatized lithosphere and emplacement of the mafic–ultramafic intrusions.

6.3. Petrogenetic model for the Huangshan intrusion

Subsequent to the closure of the Northern Tianshan Ocean and the collision of the Junggar and Central Tianshan terranes, the Northern Tianshan Orogen was overprinted by syn-collisional magmatism (Branquet et al., 2012; Laurent-Charvet et al., 2002; Song et al., 2013; Xu et al., 2003; Zhang et al., 2003). Mafic–ultramafic rocks and granitic rocks with ages of 307 Ma to 270 Ma are exposed in the Northern Tianshan Orogen. The geochemical data presented here show that the mafic magmatism progressed from lithosphere-derived melts to asthenospheric melts with time. Similar trends in other orogenic belts have been explained as the result of two geodynamic models, including slab break-off (Davies and von Blanckenburg, 1995; Song et al., 2011, 2013; Xie et al., 2012, 2014; Y.J. Mao et al., 2014) and large-scale delamination (Bird, 1979; Bonin, 2004; Kay and Kay, 1993).

The slab break-off model predicts a narrow, linear zone of magmatism with limited uplift that propagates along strike (Davies and von Blanckenburg, 1995). A key aspect of this model is the mode of deformation of the subducting plate under extension. In syn- or post-collisional orogenic belts buoyant continental lithosphere would be difficult to subduct, whereas the dense oceanic lithosphere would be easily subducted generating a large downward force and extensional deformation in the transition region forming a narrow zone of rifting (Atherton and Ghani, 2002; Davies and von Blanckenburg, 1995; von Blanckenburg and Davies, 1995). As a result of rifting during slab breakoff, hot asthenospheric mantle would upwell through the slab window and generate a thermal anomaly in the mantle wedge which in turn would cause partial melting of the asthenosphere and overriding metasomatized lithosphere, accompanied by significant crustal uplift and transient magmatic pulses (Bonin, 2004; Rogers et al., 2002; Zadde and Wortle, 2001). Alternatively, lithospheric delamination, accompanied by crustal extension, would be induced by thermal and mechanical instability of the thickened lithosphere (Marotta et al., 1998), rapid unroofing would be accompanied by hot asthenosphere upwelling and magmatic underplating (Bonin, 2004). Magmatism formed in this setting would be distributed more widely than that produced by slab break off, which would be more localized and linear (Atherton and Ghani, 2002; Davies and von Blanckenburg, 1995; von Blanckenburg and Davies, 1995).

In the Northern Tianshan a large number of mafic–ultramafic intrusions, magmatic Ni–Cu sulfide deposits, and granitoid plutons have been found in a narrow, roughly E–W zone which is not consistent with the delamination model for the Northern Tianshan (Ma et al., 2015; Song et al., 2013; Yuan et al., 2010; Zhang et al., 2014; Zhou et al., 2010). Seismic, gravity and aeromagnetic data have confirmed the existence of remnant oceanic crust in Northern Xinjiang, which has been interpreted to be subducted oceanic lithosphere (Xu et al., 2013; Z.J. Zhang et al., 2011). The linear distribution of Permian mafic–ultramafic intrusions along the Kangguer fault in the Northern Tianshan is consistent with a slab breakoff model and might also account for the formation of the mafic–ultramafic intrusions in the Central Tianshan and the Beishan Fold Belt (Chai et al., 2008; Deng et al., 2014; Song et al., 2011, 2013; Tang et al., 2011; Xia et al., 2013). As noted above, an expansive Northern Tianshan ocean existed during the Devonian–Carboniferous. The oceanic slab subducted northward to form the Dananhu arc and a mantle wedge that was modified by subducted slab-derived melt/fluid (Fig. 11a). Slab break-off at ca. 307 Ma, soon after the consolidation of Central Tianshan with the Dananhu arc, was likely responsible for the generation and subsequent eruption of the basalts in Northern Tianshan (Fig. 11b). Depending on the distance of the metasomatized enriched layer from the breakoff point, magmatism could follow breakoff at a wide range of time scales (Davies and von Blanckenburg, 1995). Assuming that slab breakoff occurred at 307 Ma, the slow increase in igneous activity can be modeled by upward migration of the thermal anomaly associated with upwelling asthenospheric mantle, with the peak in melting at around 280 Ma when the heat front reached the depth of the metasomatized layer. The upwelling hot asthenosphere would have caused partial melting in the overriding metasomatized lithosphere accompanied by significant crustal uplift (Carroll et al., 1995; Gao et al., 1998; Yang et al., 2009) and emplacement of the mafic–ultramafic intrusions (Fig. 11c). The basaltic magmatism at 307 Ma likely represents the initial stage of slab breakoff whereas the mafic–ultramafic intrusions (e.g., the Huangshan intrusion) represent the peak stage of slab breakoff, when the oceanic lithosphere was completely detached. The underplating and intraplating of basaltic magma would have provided the heat required to induce partial melting at various crustal levels and the subsequent emplacement of voluminous granitoids (Gu et al., 2006; Ma et al., 2015; Zhou et al., 2010).

7. Conclusions

The variations of the trace elements and isotope compositions of the mafic–ultramafic rocks in Northern Tianshan are consistent with primary magma produced by interactions between metasomatized lithospheric mantle and depleted asthenospheric melts. Geochemical differences between the mafic–ultramafic rocks of the Northern Tianshan and the Tarim large igneous province imply that the mafic–ultramafic rocks in the Northern Tianshan are not genetically related to the Tarim mantle plume. Slab break-off following continental collision played an important role in the Late Paleozoic tectonic evolution of the Northern Tianshan, inducing partial melting of the asthenosphere and metasomatized lithospheric mantle and the rapid emplacement of mafic–ultramafic intrusions along the Kanguer fault.

Supplementary data to this article can be found online at http://dx.doi.org/10.1016/j.lithos.2015.04.014.

Acknowledgments

We thank the management of No. 6 Geological Party, Xinjiang Bureau of Geology and Mineral Resources, for help during our field work. This study was financially supported by NSFC research grants (41303031, 41172090, 41040025), the Chinese National Science and Technology Program during the 12th Five-year Plan Period (2011BAB06B01), the Program for New Century Excellent Talents in University (Grant no. NCET-10-0324), the Fundamental Research Funds for the Central Universities (2013bhzx0015) and Open Funds from the State Key Laboratory of Ore Deposit Geochemistry, Institute of Geochemistry, Chinese Academy of Sciences (201102).

References

Atherton, M.P., Ghani, A.A., 2002. Slab breakoff: a model for Caledonian, Late Granite syn-collisional magmatism in the orthotectonic (metamorphic) zone of Scotland and Donegal, Ireland. Lithos 62, 65–85.

BGMX (Bureau of Geology and Mineral Resources of Xinjiang Uygur Autonomous Region), 1993. Regional Geology of Xinjiang Uygur Autonomous Region. Geological Publishing House, Beijing, pp. 1–841 (in Chinese with English abstract).

Bird, P., 1979. Continental delamination and the Colorado Plateau. Journal of Geophysical Research 84, 7561–7571.

Bonin, B., 2004. Do coeval mafic and felsic magmas in post-collisional to within-plate regimes necessarily imply two contrasting, mantle and crustal, sources? A review. Lithos 78, 1–24.

Branquet, Y., Gumiaux, C., Sizaret, S., Barbanson, L., Wang, B., Cluzel, D., Li, G.R., Delaunay, A., 2012. Synkinematic mafic/ultramafic sheeted intrusions: emplacement mechanism and strain restoration of the Permian Huangshan Ni–Cu ore belt (Eastern Tianshan, NW China). Journal of Asian Earth Sciences 56, 240–257.

Carroll, A.R., Graham, S.A., Hendrix, M.S., Ying, D., Zhou, D., 1995. Late Paleozoic tectonic amalgamation of northwestern China: sedimentary record of the northern Tarim, northwestern Turpan, and southern Junggar Basins. Geological Society of America Bulletin 107 (5), 571–594.

Chai, F.M., Zhang, Z.C., Mao, J.W., Dong, L.H., Zhang, Z.H., Wu, H., 2008. Geology, petrology and geochemistry of the Baishiquan Ni–Cu-bearing mafic–ultramafic intrusions in Xinjiang, NW China: implications for tectonics and genesis of ores. Journal of Asian Earth Sciences 32, 218–235.

Chen, W., Sun, S., Zhang, Y., Xiao, W.J., Wang, Y.T., Wang, Q.L., Jiang, L.F., Yang, J.T., 2005. $^{40}Ar/^{39}Ar$ geochronology of the Qiugemingtashi–Huangshan ductile shear zone in

East Tianshan, Xinjiang, NW China. Acta Geologica Sinica 79 (6), 790–804 (in Chinese with English abstract).

Chen, M.M., Tian, W., Zhang, Z.L., Pan, W.Q., Song, Y., 2010. Geochronology of the Permian basic–intermediate–acidic magma suite from Tarim, Northwest China and its geological implications. Acta Petrologica Sinica 26, 559–572 (in Chinese with English abstract).

Chen, X.J., Shu, L.S., Santosh, M., 2011. Late Paleozoic post-collisional magmatism in the Eastern Tianshan Belt, Northwest China: new insights from geochemistry, geochronology and petrology of bimodal volcanic rocks. Lithos 127, 581–598.

Chen, X.J., Shu, L.S., Santosh, M., Zhao, X.X., 2013. Island arc-type bimodal magmatism in the eastern Tianshan Belt, Northwest China: geochemistry, zircon U–Pb geochronology and implications for the Paleozoic crustal evolution in Central Asia. Lithos 168–169, 48–66.

Chung, S.L., Wang, K.L., Crawford, A.J., Kamenetsky, V.S., Chen, C.H., Lan, C.Y., Chen, C.H., 2001. High-Mg potassic rocks from Taiwan: implications for the genesis of orogenic potassic lavas. Lithos 59, 153–170.

Davies, J.H., von Blanckenburg, F., 1995. Slab break-off: a model of lithospheric detachment and its test in the magmatism and deformation of collisional orogens. Earth and Planetary Science Letters 129, 85–102.

Deng, Y.F., Song, X.Y., Chen, L.M., Cheng, S.L., Zhang, X.L., Li, J., 2011a. Features of the mantle source of the Huangshanxi Ni–Cu sulfide-bearing mafic–ultramafic intrusion, eastern Tianshan. Acta Petrologica Sinica 27 (12), 3640–3652 (in Chinese with English abstract).

Deng, Y.F., Song, X.Y., Jie, W., Chen, S.L., Li, J., 2011b. Petrogenesis of the Huangshandong Ni–Cu sulfide-bearing mafic–ultramafic intrusion, Northern Tianshan, Xinjiang: evidence from major and trace elements and Sr–Nd isotope. Acta Geologica Sinica 85 (9), 1436–1451 (in Chinese with English abstract).

Deng, Y.F., Song, X.Y., Chen, L.M., Zhou, T.F., Pirajno, F., Yuan, F., Xie, W., Zhang, D.Y., 2014. Geochemistry of the Huangshandong Ni–Cu deposit in northwestern China: implications for the formation of magmatic sulfide mineralization in orogenic belts. Ore Geology Reviews 56, 181–198.

Ellam, R.M., Hawkesworth, C.J., Menzies, M.A., Rogers, N.W., 1989. The volcanism of Southern Italy: role of subduction and the relationship between potassic and sodic alkaline magmatism. Journal of Geophysical Research 94 (B4), 4589–4601.

Elliott, T., Plank, T., Zindler, A., White, W., Bourdon, B., 1997. Element transport from slab to volcanic front at the Mariana arc. Journal of Geophysical Research-Solid Earth 102 (B7), 14991–15019.

Gao, J.F., Zhou, M.F., 2013. Generation and evolution of siliceous high magnesium basaltic magmas in the formation of the Permian Huangshandong intrusion (Xinjiang, NW China). Lithos 162–163, 128–139.

Gao, J., Li, M.S., Xiao, X.C., Tang, Y.Q., He, G.Q., 1998. Paleozoic tectonic evolution of the Tianshan Orogen, northwestern China. Tectonophysics 287, 213–231.

Gu, L.X., Zhang, Z.Z., Wu, C.Z., Wang, Y.X., Tang, J.H., Wang, C.S., Xi, A.H., Zheng, Y.C., 2006. Some problems on granites and vertical growth of the continental crust in the eastern Tianshan Mountains, NW China. Acta Petrologica Sinica 22 (5), 1103–1120 (in Chinese with English abstract).

Han, B.F., Ji, J.Q., Song, B., Chen, L.H., Li, Z.H., 2004. Zircon SHRIMP U–Pb age and geology of Kalatongke–Huangshan mafic–ultramafic complex, Xinjiang, China. Chinese Science Bulletin 49 (22), 2324–2328 (in Chinese with English abstract).

Han, C.M., Xiao, W.J., Zhao, G.C., Ao, S.J., Zhang, J.E., Qu, W.J., Du, A.D., 2010. In-situ U–Pb, Hf and Re–Os isotopic analyses of the Xiangshan Ni–Cu–Co deposit in Eastern Tianshan (Xinjiang), Central Asia Orogenic Belt: constraints on the timing and genesis of the mineralization. Lithos 120, 547–562.

Hofmann, A.W., 1988. Chemical differentiation of the Earth: the relation between mantle, continental crust, and oceanic crust. Earth and Planetary Science Letters 90, 297–314.

Hofmann, A.W., Jochum, K.P., Seufert, M., White, W.M., 1986. Nb and Pb in oceanic basalts: new constraints on mantle evolution. Earth and Planetary Science Letters 79, 33–45.

Hou, G.S., Tang, H.F., Liu, C.Q., 2006. Geochemical characteristics of the Late Paleozoic Volcanics in Jueluotage tectonic belt, eastern Tianshan and its implications. Acta Petrologica Sinica 22 (5), 1167–1177 (in Chinese with English abstract).

Hou, T., Zhang, Z.Z., Santosh, M., Encamacion, J., Zhu, J., Luo, W.J., 2014. Geochronology and geochemistry of submarine volcanic rocks in the Yamansu iron deposit, Eastern Tianshan Mountains, NW China: constraints on the metallogenesis. Ore Geology Reviews 56, 487–502.

Jahn, B.M., 2004. The Central Asian Orogenic Belt and growth of the continental crust in the Phanerozoic. Geological Society, London, Special Publications 226, 73–100.

Jahn, B.M., Wu, F.Y., Chen, B., 2000. Massive granitoid generation in Central Asia: Nd isotope evidence and implication for continental growth in the Phanerozoic. Episodes 23 (2), 82–92.

Jiang, C.Y., Zhang, P.B., Lu, D.R., Bai, K.Y., 2004a. Petrogenesis and magma source of the ultramafic rocks at Wajilitag region, western Tarim Plate in Xinjiang. Acta Petrologica Sinica 20 (6), 1433–1444 (in Chinese with English abstract).

Jiang, C.Y., Jia, C.Z., Li, L.C., Zhang, P.B., Lu, D.R., Bai, K.Y., 2004b. Source of the Fe-riched-type high-Mg magma in Mazhartag Region, Xinjiang. Acta Geologica Sinica 78 (6), 770–780 (in Chinese with English abstract).

Jiao, J.G., Tang, Z.L., Qian, Z.Z., Sun, T., Duan, J., Jiang, C., 2012. Genesis and metallogenic process of Tulargen large scale Cu–Ni sulfide deposit in eastern Tianshan area, Xinjiang. Acta Petrologica Sinica 28 (11), 3772–3786 (in Chinese with English abstract).

Jurewicz, A.J.G., Watson, E.B., 1988. Cations in olivine, Part 1: Calcium partitioning and calcium–magnesium distribution between olivines and coexisting melts, with petrologic applications. Contributions to Mineralogy and Petrology 99, 176–185.

Kamenetsky, V.S., Elburg, M., Arculus, R., Thomas, R., 2006. Magmatic origin of low-Ca olivine in subduction-related magmas: co-existence of contrasting magmas. Chemical Geology 233, 346–357.

Kay, R.W., Kay, M.S., 1993. Delamination and delamination magmatism. Tectonophysics 219, 177–189.

Laurent-Charvet, S., Charvet, J., Shu, L., Ma, R.S., Lu, H.F., 2002. Palaeozoic late collisional strike-slip deformations in Tianshan and Altay, Eastern Xinjiang, NW China. Terra Nova 14, 249–256.

Laurent-Charvet, S., Charvet, J., Monié, P., Shu, L., 2003. Late Paleozoic strike-slip shear zones in eastern central Asia (NW China): new structural and geochronological data. Tectonics 22 (2). http://dx.doi.org/10.1029/2001TC901047.

Li, S.G., 1995. Implications of ε_{Nd}-La/Nb, Ba/Nb, Nb/Th diagrams to mantle heterogeneity-classification of island arc basalts and decomposition of EMII component. Chinese Journal of Geochemistry 14 (2), 117–127.

Li, D.H., Bao, X., Zhang, B., Han, Z., Lan, G., Zheng, Z., et al. 1989. Investigation of geology, geophysics and geochemistry of the Huangshan-Cu–Ni metallogenic belt for mineral exploration, unpublished report by National 305 project office in Xinjiang. 1–418 (in Chinese).

Li, J.Y., Wang, K.Z., Sun, G.H., Mo, S.G., Li, W.Q., Yang, T.N., Gao, L.M., 2006a. Paleozoic active margin slices in the southern Turfan Hami basin: geological records of subduction of the Paleo Asian Ocean plate in central Asian regions. Acta Petrologica Sinica 22 (5), 1087–1102 (in Chinese with English abstract).

Li, J.Y., Song, B., Wang, K.Z., Li, Y.P., Sun, G.H., Qi, D.Y., 2006b. Permian mafic–ultramafic complexes on the Southern margin of the Tu–Ha basin, east Tianshan mountains: geological records of vertical crustal growth in Central Asia. Acta Geoscientica Sinica 27 (5), 424–446 (in Chinese with English abstract).

Li, C.S., Thakurta, J., Ripley, E.M., 2012. Low-Ca contents and kink-banded textures are not unique to mantle olivine: evidence from the Duke Island Complex, Alaska. Mineralogy and Petrology 104, 147–153.

Libourel, G., 1999. Systematics of calcium partitioning between olivine and silicate melt: implications for melt structure and calcium content of magmatic olivines. Contributions to Mineralogy and Petrology 136, 63–80.

Ma, R.S., Wang, C.Y., Ye, S.F., Liu, G.B., 1993. Tectonic framework and crustal evolution of the Eastern Tianshan. Nanjing University Press (in Chinese).

Ma, X.X., Shu, L.shu, Meert, J.G., 2015. Early Permian slab breakoff in the Chinese Tianshan belt inferred from the post-collisional granitoids. Gondwana Research 27, 228–243. http://dx.doi.org/10.1016/j.gr.2013.09.018.

Mao, Y.J., 2014. Petrogenesis and Ore Genesis of the Multi-stage Mafic–Ultramafic Intrusions in the Huangshan Ni–Cu Camp, Eastern Tianshan, Southern Central Asian Orogenic Belt. (Ph.D. Dissertation), University of Chinese Academy of Sciences, Beijing, pp. 1–178 (in Chinese with English abstract).

Mao, J.W., Pirajno, F., Zhang, Z.H., Chai, F.M., Yang, J.M., Wu, H., Chen, S.P., Cheng, S.L., Zhang, C.Q., 2006. Late Variscan post-collisional Cu–Ni sulfide deposits in East Tianshan and Altay in China: principal characteristics and possible relationship with mantle plume. Acta Geologica Sinica 80 (7), 927–942 (in Chinese with English abstract).

Mao, J.W., Pirajno, F., Zhang, Z.H., Chai, F.M., Wu, H., Chen, S.P., Chen, L.S., Yang, J.M., Zhang, C.Q., 2008. A review of the Cu–Ni sulphide deposits in the Chinese Tianshan and Altay orogens (Xinjiang Autonomous Region, NW China): principal characteristics and ore-forming processes. Journal of Asian Earth Sciences 32 (2-4), 184–203.

Mao, Q.G., Xiao, W.J., Fang, T.H., Windley, B.F., Sun, M., Ao, S.J., Zhang, J.E., Huang, X.K., 2014a. Geochronology, geochemistry and petrogenesis of Early Permian alkaline magmatism in the Eastern Tianshan: implications for tectonics of the Southern Altaids. Lithos 190–191, 37–51.

Mao, Y.J., Qin, K.Z., Li, C., Xue, S.C., Ripley, E.M., 2014b. Petrogenesis and ore genesis of the Permian Huangshanxi sulfide ore-bearing mafic–ultramafic intrusion in the Central Asian Orogenic Belt, western China. Lithos 200, 111–125.

Marini, J.C., Chauvel, C., Maury, R.C., 2005. Hf isotope compositions of northern Luzon arc lavas suggest involvement of pelagic sediments in their source. Contributions to Mineralogy and Petrology 149, 216–232.

Marotta, A.M., Fernandez, M., Sabadini, R., 1998. Mantle unrooting in collisional settings. In: Vauchez, A., Meissner, R. (Eds.), Continents and their mantle roots. Tectonophysics 296, pp. 31–46.

McDonough, W.F., Sun, S.S., 1995. Composition of the Earth. Chemical Geology 120, 223–253.

Niu, Y.L., 2005. Generation and evolution of basaltic magmas: some basic concepts and a new view on the origin of Mesozoic–Cenozoic basaltic volcanism in eastern China. Geological Journal of China Universities 11 (1), 9–46.

Pearce, J.A., 1982. Trace elements characteristics of lavas from destructive plate boundaries. In: Thorpe, R.S. (Ed.), Andesites: Orogenic Andesites and Related Rocks. Wiley, New York, pp. 525–548.

Pearce, J.A., Peate, D.W., 1995. Tectonic implications of the composition of volcanic arc magmas. Annual Review of Earth and Planetary Science Letters 23, 251–285.

Pearce, J.A., Baker, P.E., Harvey, P.K., Luff, I.W., 1995. Geochemical evidence for subduction fluxes, mantle melting and fractional crystallization beneath the South Sandwich island arc. Journal of Petrology 36 (4), 1073–1109.

Pirajno, F., Mao, J.W., Zhang, Z.H., Chai, F.M., 2008. The association of mafic–ultramafic intrusions and A-type magmatism in the Tian Shan and Altay orogens, NW China: implications for geodynamic evolution and potential for the discovery of new ore deposits. Journal of Asian Earth Sciences 32 (2-4), 165–183.

Plank, T., Langmuir, C.H., 1998. The chemical composition of subducting sediment and its consequences for the crust and mantle. Chemical Geology 145 (3-4), 325–394.

Qi, L., Hu, J., Gregoire, D.C., 2000. Determination of trace elements in granites by inductively coupled plasma mass spectrometry. Talanta 51 (3), 507–513.

Qin, K.Z., Fang, T.H., Wang, S.L., Zhu, B.Q., Feng, Y.M., Yu, H.F., Xiu, Q.Y., 2002. Plate tectonics division, evolution and metallogenic settings in eastern Tianshan mountains, NW-China. Xinjiang Geology 20 (4), 302–308 (in Chinese with English abstract).

Qin, K.Z., Zhang, L.C., Xiao, W.J., Xu, X.W., Yan, Z., Mao, J.W., 2003. Overview of major Au, Cu, Ni and Fe deposits and metallogenic evolution of the eastern Tianshan Mountains, Northwestern China. In: Mao, J.W., Goldfarb, R., Seltmann, R., Wang, D.H., Xiao, W.J., Hart, C. (Eds.), Tectonic evolution and metallogeny of the Chinese Altay and Tianshan. London: IAGOD Guidebook Series 10, pp. 227–248.

Qin, K.Z., Sun, B.X., Sakyi, P.A., Tang, D.M., Li, X.H., Sun, H., Xiao, Q.H., Liu, P.P., 2011. SIMS zircon U–Pb geochronology and Sr–Nd isotopes of Ni–Cu-bearing mafic–ultrafic intrusions in Eastern Tianshan and Beishan in correlation with flood basalts in Tarim basin (NW China): constraints on a ca. 280 Ma mantle plume. American Journal of Science 311 (3), 237–260.

Rogers, R.D., Kárason, H., van der Hilst, R.D., 2002. Epeirogenic uplift above a detached slab in northern Central America. Geology 30, 1031–1034.

Rudnick, R., Fountain, D., 1995. Nature and composition of the continental crust: a lower crustal perspective. Reviews of Geophysics 33 (3), 267–309.

San, J.Z., Qin, K.Z., Tang, D.M., Su, B.X., Sun, H., Xiao, Q.H., Liu, P.P., Cao, M.J., 2010. Precise zircon U–Pb ages of Tulargen large Cu–Ni-ore bearing mafic–ultramafic complex and their geological implications. Acta Petrologica Sinica 26 (10), 3027–3035 (in Chinese with English abstract).

Sengör, A.M.C., Natal'in, B.A., Burtman, V.S., 1993. Evolution of the Altaid tectonic collage and Paleozoic crustal growth in Asia. Nature 364, 299–307.

Shu, L.S., Charvet, J., Guo, L., Lu, H., Laurent-Charvet, S., 1999. A large-scale Paleozoic dextral ductile strike-slip zone: The Aqqikkudug–Weiya zone along the northern margin of the Central Tianshan belt, Xinjiang, NW China: new structural and geochronological data. Acta Geologica Sinica 73, 148–162.

Shu, L.S., Wang, B., Zhu, W.B., Guo, Z.J., Charvet, J., Zhang, Y., 2010. Timing of initiation of extension in the Tianshan, based on structural, geochemical and geochronological analyses of bimodal volcanism and olistostrome in the Bogda Shan (NW China). International Journal of Earth Sciences (Geologische Rundschau) http://dx.doi.org/10.1007/s00531-010-0575-5.

Song, X.-Y., Li, X.-R., 2009. Geochemistry of the Kalatongke Ni–Cu-(PGE) sulfide deposit, NW China: implications for the formation of magmatic sulfide mineralization in a post-collisional environment. Mineralium Deposita 44, 303–327.

Song, X.-Y., Xie, W., Deng, Y.F., Crawford, A.J., Zheng, W.Q., Zhou, G.F., Deng, G., Chen, S.L., Li, J., 2011. Slab break-off and the formation of Permian mafic–ultramafic intrusions in southern margin of Central Asian Orogenic Belt, Xinjiang, NW China. Lithos 127 (1-2), 128–143.

Song, X.-Y., Chen, L.-M., Deng, Y.F., Xie, W., 2013. Syncollisional tholeiitic magmatism induced by asthenosphere upwelling owing to slab detachment at the southern margin of the Central Asian Orogenic Belt. Journal of the Geological Society, London 170, 941–950.

Su, B.X., Qin, K.Z., Sakyi, P.A., Li, X.H., Yang, Y.H., Sun, H., Tang, D.M., Liu, P.P., Xiao, Q.H., Malaviarachchi, S.P., 2011. U–Pb ages and Hf–O isotopes of zircons from Late Paleozoic mafic–ultramafic units in the southern Central Asian Orogenic Belt: tectonic implications and evidence for an Early–Permian mantle plume. Gondwana Research 20 (2-3), 516–531.

Su, B.X., Qin, K.Z., Su, H., Tang, D.M., Sakyi, P.A., Chu, Z.Y., Liu, P.P., Xiao, Q.H., 2012. Subduction-induced mantle heterogeneity beneath Eastern Tianshan and Beishan: Insights from Nd–Sr–Hf–O isotopic mapping of Late Paleozoic mafic–ultramafic complexes. Lithos (134-135), 41–51.

Sun, S.S., McDonough, W., 1989. Chemical and isotopic systematics of oceanic basalts: implications for mantle composition and processes. Geological Society, London, Special Publications 42 (1), 313–345.

Sun, T., Qian, Z.Z., Li, C.S., Xia, M.Z., Yang, S.H., 2013a. Petrogenesis and economic potential of the Erhongwa mafic–ultramafic intrusion in the Central Asian Orogenic Belt, NW China: constraints from olivine chemistry, U–Pb age and Hf isotopes of zircons, and whole-rock Sr–Nd–Pb isotopes. Lithos 182–183, 185–199.

Sun, T., Qian, Z.Z., Deng, Y.F., Li, C.S., Song, X.Y., Tang, Q.Y., 2013b. PGE and isotope (Hf–Sr–Nd–Pb) constraints on the origin of the Huangshandong magmatic Ni–Cu sulfide deposit in the Central Asian Orogenic Belt, Northwestern China. Economic Geology 108, 1849–1864.

Tang, D.M., Qin, K.Z., Li, C.S., Qi, L., Su, B.X., Qu, W.J., 2011. Zircon dating, Hf–Sr–Nd–Os isotopes and PGE geochemistry of the Tianyu sulfide-bearing mafic–ultramafic intrusion in the Central Asian Orogenic Belt, NW China. Lithos 126, 84–98.

Tang, D.M., Qin, K.Z., Su, B.X., Sakyi, P.A., Liu, Y.S., Mao, Q., Santosh, M., Ma, Y.G., 2013. Magma source and tectonics of the Xiangshanzhong mafic–ultramafic intrusion in the Central Asian Orogenic Belt, NW China, traced from geochemical and isotopic signatures. Lithos 170–171, 144–163.

Thakurta, J., Ripley, E.M., Li, C.S., 2008. Geochemical constraints on the origin of sulfide mineralization in the Duke Island Complex, southeastern Alaska. Geochemistry, Geophysics, Geosystems 9 (7), Q07003. http://dx.doi.org/10.1029/2008GC001982.

Turner, S.P., Foden, J., 2001. U, Th and Ra disequilibria, Sr, Nd and Pb isotope and trace element variations in Sunda arc lavas: predominance of a subducted sediment component. Contributions to Mineralogy and Petrology 142, 43–57.

Turner, S.P., Hawkesworth, C., Rogers, N., Bartlett, J., Worthington, T., Hergt, J., Pearce, J., Smith, I., 1997. $^{238}U–^{230}Th$ disequilibria, magma petrogenesis, and flux rates beneath the depleted Tonga–Kermadec island arc. Geochimica et Cosmochimica Acta 61 (22), 4855–4884.

von Blanckenburg, F., Davies, J.H., 1995. Slab breakoff: a model for syncollisional magmatism and tectonics in the Alps. Tectonics 14 (1), 120–131.

Wang, R.M., Liu, D.Q., Ying, D.T., et al., 1987. Cu–Ni sulfide deposits in the Tudun–Huangshan region, Hami, Xinjiang: Genet controls exploration implications. Miner Rocks 7, 1–152 (in Chinese).

Wartes, M.A., Carroll, A.R., 2002. Permian sedimentary record of the Turpan–Hami basin and adjacent regions, northwest China: constraints on postamalgamation tectonic evolution. Geological Society of America Bulletin 114 (2), 131–152.

Wilson, M., 1989. Igneous Petrogenesis. Unwin Hyman, London, pp. 1–466.

Windley, B.F., Alexeiev, D., Xiao, W.J., Kröner, A., Badarch, G., 2007. Tectonic models for accretion of the Central Asian Orogenic Belt. Journal of the Geological Society of London 164, 31–47.

Xia, M.Z., Jiang, C.Y., Qian, Z.Z., Sun, T., Xia, Z.D., Lu, R.H., 2008. Geochemistry and petrogenesis for Hulu intrusion in East Tianshan, Xinjiang. Acta Petrologica Sinica 24 (12), 2749–2760 (in Chinese with English abstract).

Xia, M.Z., Jiang, C.Y., Li, C.S., Xia, Z.D., 2013. Characteristics of a newly discovered Ni–Cu sulfide deposit hosted in the Poyi ultramafic intrusion, Tarim Craton, NW China. Economic Geology 108, 1865–1878.

Xiao, W.J., Zhang, L.C., Qin, K.Z., Sun, S., Li, J.L., 2004. Paleozoic accretionary and collisional tectonics of the Eastern Tianshan (China): implications for the continental growth of central Asia. American Journal of Science 304, 370–395.

Xiao, W.J., Han, C.M., Yuan, C., Sun, M., Lin, S.F., Chen, H.L., Li, Z.L., Li, J.L., Sun, S., 2008. Middle Cambrian to Permian subduction-related accretionary orogenesis of Northern Xinjiang, NW China: implications for the tectonic evolution of central Asia. Journal of Asian Earth Sciences 32 (2-4), 102–117.

Xiao, W.J., Windley, B.F., Huang, B.C., Han, C.M., Yuan, C., Chen, H.L., Sun, M., Sun, S., Li, J.L., 2009. End-Permian to mid-Triassic termination of the accretionary processes of the southern Altaids: implications for the geodynamic evolution, Phanerozoic continental growth, and metallogeny of Central Asia. International Journal of Earth Sciences 98, 1189–1217.

Xie, W., Song, X.Y., Deng, Y.F., Wang, Y.S., Ba, D.H., Zheng, W.Q., Li, X.B., 2012. Geochemistry and petrogenetic implications of a Late Devonian mafic–ultramafic intrusion at the southern margin of the Central Asian Orogenic Belt. Lithos 144–145, 209–230.

Xie, W., Song, X.Y., Chen, L.M., Deng, Y.F., Zheng, W.Q., Wang, Y.S., Ba, D.H., Zhang, X.Q., Luan, Y., 2014. Geochemistry insights on the genesis of the subduction-related Heishan magmatic Ni–Cu–(PGE) deposit in Gansu, NW China, at the Southern Margin of the Central Asian Orogenic Belt. Economic Geology 109, 1563–1583.

Xu, X.W., Ma, T.L., Sun, L.Q., Cai, X.P., 2003. Characteristics and dynamic origin of the large-scale Jiaoluotage ductile compressional zone in the eastern Tianshan Mountains, China. Journal of Structural Geology 25, 1901–1915.

Xu, Q.Q., Ji, J.Q., Zhao, L., Gong, J.F., Zhou, J., He, G.Q., Zhong, D.L., Wang, J.D., Griffiths, L., 2013. Tectonic evolution and continental crust growth of Northern Xinjiang in northwestern China: remnant ocean model. Earth-Science Reviews 126, 178–205.

Yang, T.N., Li, J.Y., Wang, Y., Deng, Y.X., 2009. Late Early Permian (266 Ma) N–S compressional deformation of the Turfan basin, NW China: the cause of the change in basin pattern. International Journal of Earth Sciences 98, 1311–1324.

Yang, Y.H., Zhang, F.H., Chu, Z.Y., Xie, X.W., Wu, F.Y., 2010. Combined chemical separation of Lu, Hf, Rb, Sr, Sm and Nd from a single rock digest and precise and accurate isotope determinations of Lu–Hf, Rb–Sr and Sm–Nd isotope systems using Multi-Collector ICP-MS and TIMS. International Journal of Mass Spectrometry 290, 120–126.

Yu, X., Yang, S.F., Chen, H.L., Chen, Z.Q., Li, Z.L., Batt, G.E., Li, Y.Q., 2011. Permian flood basalts from the Tarim Basin, Northwest China: SHRIMP zircon U–Pb dating and geochemical characteristics. Gondwana Research 20, 485–497.

Yuan, F., Zhou, T.F., Fan, Y., Tan, L.G., David, C., Sebastien, M., Wang, Q.M., Wang, W.J., 2007. LA-ICPMS U–Pb age of zircon from basalt of Matoutan Group in Shilipo native copper mineralized area, Eastern Tianshan, Xinjiang. Acta Petrologica Sinica 23, 1973–1980 (in Chinese with English abstract).

Yuan, C., Sun, M., Wilde, S., Xiao, W.J., Xu, Y.G., Long, X.P., Zhao, G.C., 2010. Post-collisional plutons in the Balikun area, East Chinese Tianshan: evolving magmatism in response to extension and slab break-off. Lithos 119 (3-4), 269–288.

Zadde, D.M.A., Wortle, M.J.R., 2001. Shallow slab detachment as a transient source of heat at midlithospheric depths. Tectonics 20, 868–882.

Zhang, L.C., Shen, Y.C., Ji, J.S., 2003. Characteristics and genesis of Kanggur gold deposit in the eastern Tianshan mountains, NW China: evidence from eology, isotope distribution and chronology. Ore Geology Reviews 23, 71–90.

Zhang, L.C., Xiao, W.J., Qin, K.Z., Zhang, Q., 2006. The adakite connection of the Tuwu-Yandong copper porphyry belt, eastern Tianshan, NW China: trace element and Sr–Nd–Pb isotope geochemistry. Mineralium Deposita 41 (2), 188–200.

Zhang, C., Li, X., Li, Z., Ye, H., Li, C., 2008. A Permian layered intrusive complex in the western Tarim Block, northwestern China: product of a ca. 275-Ma mantle plume? The Journal of Geology 116 (3), 269–287.

Zhang, M.J., Li, C.S., Fu, P.E., Hu, P.Q., Ripley, E.M., 2011a. The Permian Huangshanxi Cu–Ni deposit in western China: intrusive–extrusive association, ore genesis, and exploration implications. Mineralium Deposita 46 (2), 153–170.

Zhang, Z.J., Yang, L.Q., Teng, J.W., Badal, José, 2011b. An overview of the earth crust under China. Earth-Science Reviews 104, 143–166.

Zhang, D.Y., Zhou, T.F., Yuan, F., Jowitt, S.M., Fan, Y., Liu, S., 2012. Source, evolution and emplacement of Permian Tarim Basalts: evidence from U–Pb dating, Sr–Nd–Pb–Hf isotope systematics and whole rock geochemistry of basalts from the Keping area, Xinjiang Uygur Autonomous region, northwest China. Journal of Asian Earth Sciences 49, 175–190.

Zhang, D.Y., Zhou, T.F., Yuan, F., Fiorentini, M.L., Said, N., Lu, Y.J., Pirajno, F., 2013. Geochemical and isotopic constraints on the genesis of the Jueluotage native copper mineralized basalt, Eastern Tianshan, Northwest China. Journal of Asian Earth Sciences 73, 317–333.

Zhang, D.Y., Zhou, T.F., Yuan, F., Fan, Y., Deng, Y.F., Xu, C., Zhang, R.F., 2014. Genesis of Permian Granites along the Kangguer Shear Zone, Jueluotage area, Northwest China: geological and geochemical evidence. Lithos 198-199, 141–152.

Zhou, M.F., Lesher, C.M., Yang, Z.X., Li, J.W., Sun, M., 2004. Geochemistry and petrogenesis of 270 Ma Ni–Cu–(PGE) sulfide–bearing mafic intrusions in the Huangshan District, eastern Xinjiang, northwest China; implications for the tectonic evolution of the Central Asian orogenic belt. Chemical Geology 209 (3-4), 233–257.

Zhou, D.W., Liu, Y.Q., Xin, X.J., Hao, J.R., Dong, Y.P., Ouyang, Z.J., 2006. Formation of the Permian basalts and implications of geochemical tracing for paleo-tectonic setting and regional tectonic background in the Turpan–Hami and Santanghu basins, Xinjiang. Science in China, Series D Earth Sciences 49, 584–596 (in Chinese with English abstract).
Zhou, M.F., Zhao, J.H., Jiang, C.Y., Gao, J.F., Wang, W., Yang, S.H., 2009. OIB-like, heterogeneous mantle sources of Permian basaltic magmatism in the western Tarim Basin, NW China: implications for a possible Permian large igneous province. Lithos 113, 583–594.
Zhou, T.F., Yuan, F., Zhang, D.Y., Fan, Y., Liu, S., Peng, M.X., Zhang, J.D., 2010. Geochronology, tectonic setting and mineralization of granitoids in Jueluotage area, eastern Tianshan, Xinjiang. Acta Petrologica Sinica 26 (2), 478–502 (in Chinese with English abstract).